Nonlinear modal synthesis for analyzing structures with a frictional interface using a generalized Masing model

Xing-Rong Huang, Louis Jézéquel, Sébastien Besset, Lin Li, Olivier Sauvage

Nonlinear modal synthesis for analyzing structures with a frictional interface using a generalized Masing model

Xing-Rong Huang[a, *], Louis Jézéquel[b], Sébastien Besset[b], Lin Li[c], Olivier Sauvage[d]

[a] *Ecole Centrale de Pékin, Beihang University, 37, Xueyuan Road, 100191 Beijing, China*
[b] *Laboratoire de Tribologie et Dynamique des Systemes, Ecole Centrale de Lyon, 36, Avenue Guy de Collongues, 69134 Ecully, France*
[c] *School of Energy and Power Engineering, Beihang University, 37, Xueyuan Road, 100191 Beijing, China*
[d] *Groupe PSA, Scientific and Future Technologies Department/StelLab, F-78943 Vélizy Villacoublay Cedex, France*

ARTICLE INFO

Handling Editor: L.N. Virgin

Keywords:
Nonlinear mode
Modal synthesis
Complex modes
Branch modes
Reduced model
Dry friction
Masing model
Steady state response

ABSTRACT

The objective of this paper is to present a numerical scheme for applying nonlinear modal synthesis to study the dynamic performance of assembled structures with a frictional interface. A generalized Masing model is introduced to describe the frictional mechanism in steady state to enable obtaining the harmonic components of the friction force. By employing the concept of nonlinear modes based on normal form theory, a reduction technique based on branch modes can be applied to obtain a reduced order model. Both complex nonlinear modes and real nonlinear modes depending on the modal amplitude are used in the nonlinear modal synthesis approach, leading to a particular damping term representing energy dissipation due to friction. The implementation of the nonlinear modal synthesis combined with the generalized Masing model provides a simple, fast and efficient numerical method for describing the nonlinear performance of structures with dry friction devices. The proposed approach is applied to three increasingly complex case studies. Numerical simulations are carried out to demonstrate the efficiency and reliability of the method.

1. Introduction

The dynamic behavior of assembled structures such as vehicles and large lightweight space structures is significantly influenced by the structural connections. Damping treatments must be applied to these structures to mitigate vibration problems. High temperatures and high rotation speeds prevent traditional damping treatments in certain aerodynamic applications. If no special damping treatment is applied to these structures, dry friction damping at bolted joints may be the most important damping source [1,2]. Since dry friction devices are usually introduced to reduce the resonant responses of the systems, it is very important to model and simulate these friction devices in order to identify the optimal structural parameters during the pre-design process. The introduction of frictional devices renders the system nonlinear and the computational cost of simulations is thus considerable. It is therefore necessary to

* Corresponding author. Ecole Centrale de Pékin, Beihang University, 37, Xueyuan Road, 100191 Beijing, China.
Email address: huangxingrong@buaa.edu.cn (X-R Huang)

use reduction techniques for simulation, and various studies on developing efficient strategy for analyzing frictional systems have been conducted [3,4]. The most important objective of this work is to provide a simple and efficient numerical method for implementing reduced methods in nonlinear structural dynamics due to frictional devices. The originality of the proposed method lies in the generalized nonlinear component mode synthesis with normal form theory for solving problems including frictional phenomena.

Friction models play a fundamental role in the simulation of mechanical systems with dry friction. The choice of friction model depends on the real usage of friction devices and the physical parameters characterizing the contact surface. Various adapted models have been developed to describe friction phenomena in nonlinear dynamics [5]. The Coulomb model is a basic exemple that provides a threshold value for the friction force, and above which motion can be stimulated. However, complex phenomena [1] such as hysteresis, stick-slip and the Stribeck effect can be exhibited by dry friction. To analyze these phenomena, other dynamic models [6] such as the Dahl's model [7], the LuGre model [8], and the Leuven's model [9] have been developed with velocity dependent functions and additional damping terms associated with micro- and macro- displacements. Each model has its own distinctive advantages and disadvantages, although none of them can claim general validity. Another important issue is to explore an appropriate method for integrating the friction model in the numerical simulation scheme. Based on the principle that the friction model must be as simple as possible and as accurate as necessary, we choose to investigate the generalized Zener model, which is one of the simplest viscoelastic models reflecting the behavior of real solid materials [10,11].

The stick-slip nature of the friction damper plays a crucial role in energy dissipation [12]. For engineering applications involving dry friction, the dissipated energy is represented by the surface surrounded by the hysteresis loop. Various approaches and mathematical models [13–17] are available for describing hysteresis, and Masing's model is chosen for its proven efficiency in describing hysteretic behavior of mechanical problems Fougeres, 1989 [18,19]. Masing [20] proposed a rule for cyclically stabilized hysteretic behavior. Masing's hypothesis is that the unloading and reloading branches of the steady state hysteretic response of the system are geometrically similar to the initial-loading curve. Based on this assumption, the nonlinear force induced by dry friction in steady state can be calculated with the initial-loading curve.

The frictional system exhibits stick-slip behavior and the friction force varies with the physical displacement of the friction point. In particular, the overall damping level and the amplitude of stick-slip motion strongly depend on the friction point [21]. To analyze these nonlinear structures, time integration methods [22], such as the Newmark method and the Runge-Kutta method, can provide quite accurate results, although they are time-consuming, especially when analyzing large nonlinear systems containing numerous degrees of freedom (dofs) [23]. These time integration methods can be very inefficient if one is interested only in the steady state response, since hundreds of forcing periods can be taken into account until the transient response dies out. Moreover, certain methods may induce large discrepancies if time steps are not properly chosen. The harmonic balance method (HBM) is adapted to compute nonlinear response functions in the frequency domain, the basic idea of which is to decompose the solution into Fourier series and to solve the equations linking Fourier coefficients [24,25]. Industrial systems are in generally large-scale and their discrete models contain a large number of dofs. However, these classical methods cannot be used to optimize the geometry of these nonlinear systems. Therefore, fast and efficient numerical methods are required to optimize the pre-design process of industrial systems.

Based on the normal form theory, Rosenberg has proposed the concept of nonlinear normal modes (NNMs) to study nonlinear systems [26]. He stated that resonance occurs in the neighborhood of normal mode vibration regardless of whether the system is linear or nonlinear; the response near the main resonance can be represented by this main resonant mode. The NNMs concept has been further developed and extended by various authors, resulting in the energy-based formulation [27], invariant manifolds [28], the asymptotic approach involving numerical techniques [29], and the superposition technique in which the steady state response is considered to be a linear combination of single nonlinear mode responses [30–32]. Based on the NNMs concept, Szemplinska-Stupnicka [33] validated a single nonlinear mode approach with approximate methods such as the averaging method and the asymptotic method [34]. A comprehensive review of reduction techniques in nonlinear dynamics was presented in Touzé and Amabili [29]; Lülf et al. [35]; Festjens et al. [36]; Mohammadali and Ahmadian [37]. Under the assumption that the superposition technique and the NNMs concept can be applied to the nonlinear systems, component mode synthesis methods [38] can be applied to obtain a reduced order model. Branch mode analysis has proven to be powerful tool for analyzing assembled mechanical structures by condensing the modes of the structure on their interfaces by using the static response modes of the global structure [39–41].

In this paper, extensions of nonlinear modal synthesis are conducted to study assembled structures that incorporate the hysteresis effects of dry friction. The originality of this method is that it combines the generalized Masing model with the nonlinear modal synthesis based on branch modes. A general formulation integrating friction force is developed by combining the NNMs concept and the generalized Masing model. Reduction techniques are integrated in the modal synthesis approach. Two modal synthesis approaches are described: the real modal synthesis and the complex modal synthesis. The first technique consists in using real modes in modal synthesis: the friction damping is obtained by evaluating the ratio of energy dissipation and maximum energy per cycle. The second technique concerns the complex modes: the friction damping is obtained by calculating the ratio of the imaginary and real part of the

eigenvalue. Compared to real modal synthesis, the complex modal synthesis method includes the friction damping term in the resulting set of nonlinear equations to be solved. This makes it possible to directly extract the nonlinear properties of the dry friction damper without having to recalculate the energy dissipation. Nonlinear modal parameters, *i.e.* mode shapes, natural frequencies and damping ratios, are obtained by performing iterative numerical methods with the reduced order model. Frictional impact phenomena and steady state responses are analyzed by using the nonlinear modal parameters extracted using the proposed method. Forced responses are then computed based on these modal parameters.

The outline of the paper the following. First, Section 2 describes the generalized Masing model, which allows calculating the harmonic components of the frictional force in the following analysis. Then, Section 3 presents the nonlinear modal synthesis along with the computation of the steady state responses of the nonlinear system. The reduction technique based on branch modes is presented. The extraction of the friction damping ratio by using complex and real nonlinear modes are highlighted. These numerical methods are used in Section 4 which presents case studies that illustrate and validate the proposed method. Lastly, general conclusions and the outlook are presented in Section 5.

2. Description of the generalized Masing model

In order to characterize the steady state hysteresis behavior further employed in the modal analysis, Masing's rule is employed to illustrate the friction-displacement relation curve [20]. Assuming that the initial loading is described by the friction-displacement curve:

$$M(f,x)=0 \tag{1}$$

According to Masing's rule, the initial loading takes place up to the maximum stress, corresponding to the maximum shear strain, after which the model was unloaded to the minimum stress and reloaded back to the maximum [18]. The reloading curve can be obtained by scaling the initial loading by a factor of 2 both along the x and f axes, as shown in Eq. (2). The unloading curve has the same shape as the reloading one, rotated by 180°.

$$M\left(\frac{f-f_m}{2},\frac{x-x_m}{2}\right)=0 \tag{2}$$

The choice of friction model depends on the concrete frictional phenomena under consideration. To understand the friction phenomena in engineering, let us examine a turbomachinery blade with properly designed interfaces [42]. Dry friction on the interface provides both displacement and velocity dependent damping. Two forces are observed in this case: a pressure force that is normal to the frictional interface and an in-plane restoring force which opposes the transverse displacement of the damping node. Various dry friction models can be extended to a generalized Masing model by using Masing's rule. A simple friction model is the bilinear damper model, also called the Zener model. The general lumped-parameter system with friction damper using the Zener model is illustrated by Fig. 1. The Zener model is based on the elasto-plastic or macro-slip bilinear element, described by the static stiffness k_t, the kinetic stiffness k_d, the friction coefficient μ_d and the threshold displacement x_d after which slip occurs. The corresponding friction law reads:

$$f=\begin{cases}(k_d+k_t)\,x & x\in[0,x_d]\\ k_t x+k_d x_d & x\in[x_d,+\infty]\end{cases} \tag{3}$$

Applying Masing's rule, the expressions of the corresponding reloading curve and unloading curve are given by Eq. (4). f_{m_1} corresponds to the unloading curve and f_{m_2} corresponds to the reloading curve. The hysteresis loop of this bilinear model using Masing's rule is presented in Fig. 2. The harmonic components of the dry friction force over one

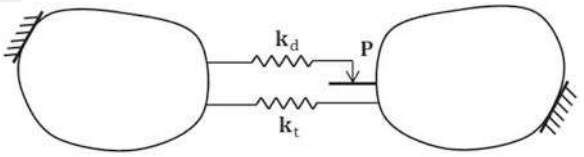

Fig. 1. Lumped-parameter system with dry friction modeled by one damper.

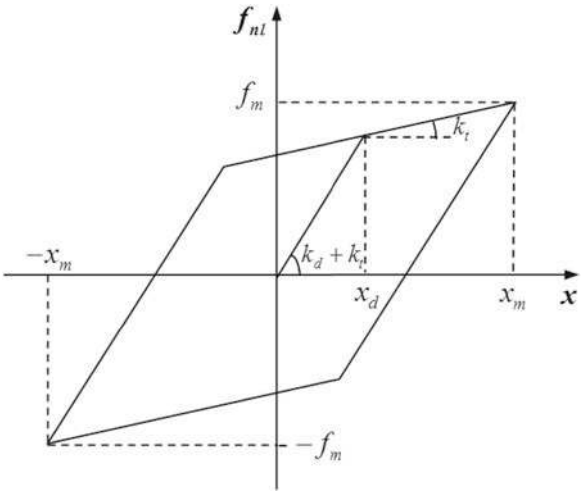

Fig. 2. The hysteresis loop of the bilinear model.

steady state period can then be determined using the alternating frequency/time technique.

$$f = \begin{cases} f_{m_1}(x) & = 2f\left(\frac{x+x_m}{2}\right) - f_m \quad x_m \to -x_m \\ f_{m_2}(x) & = -2f\left(\frac{-x+x_m}{2}\right) + f_m \quad -x_m \to x_m \end{cases} \tag{4}$$

This single bilinear hysteresis element is often used for modeling friction damping in systems due to its low computation cost and the simplicity of calibrating the damped model against experimental data. The drawback of this model is that it cannot capture the full richness of the frequency response with more complicated friction phenomena [1]. However, when these devices are placed in parallel, abundant friction phenomena can be observed and an infinity of macro-slip dampers organized in parallel yields a generalized Zener model, as shown in Fig. 3.

Rheological models similar to the generalized Zener model has already been used to represent the hysteresis behavior of cyclically deformed elastoplastic materials in Fougeres and Sidoroff [36]; and to perform mathematical investigations in Bastien et al. [13]. The physics underlying this model can be understood by imagining friction as a contact scenario involving a large population of interacting asperities subject to such phenomenological mechanisms [43]. The first dampers slip after several initial transient oscillations and then other dampers slip successively after the first dampers. Therefore, the hysteresis losses take place as soon as the first slip occurs. Substantial stick-slip can be observed providing two functionalities: the tuned absorber - frictional energy dissipation due to the slip-state of certain damping elements; the damper - resonant response amplitude reduction due to the stick-state of other damping elements. This model provides a very substantial stick-slip design region for physically reasonable damper stiffness values, corresponding to the natural frequency shifts observed during sticking. More specifically, let us assume that n dampers are set in parallel to interpolate the generalized Masing model, each macro-slip element contains three characterizing parameters, the dynamic stiffness k_{d_j}, the threshold displacement x_j and the threshold force f_{d_j}:

$$\left(x_0, f_{d_0}\right), \left(x_2, f_{d_2}\right) \cdots \left(x_j, f_{d_j}\right) \cdots \left(x_n, f_{d_n}\right)$$

The maximum threshold when all the dampers start to slip is x_g. The threshold of damper-j after which it starts to slip is determined by the corresponding ratio $r_j \in [0,1]$:

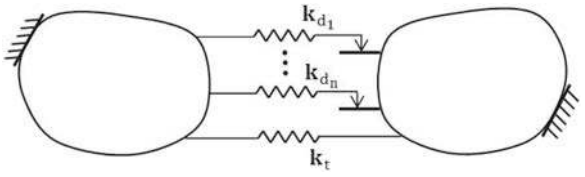

Fig. 3. Lumped-parameter system with dry friction modeled by an infinity of dampers.

$$r_j = \frac{k_{d_j}}{k_{d_1} + k_{d_2} + \cdots + k_{d_n}} \tag{5}$$

$$x_1 = r_1 x_g, x_2 = r_2 x_g, \cdots, x_j = r_j x_g, \cdots, x_n = r_n x_g \tag{6}$$

Consequently, the nonlinear force f_j corresponding to each threshold value x_j of damper-j is given as follows:

$$\begin{aligned} f_{d_1} &= x_1 \left[k_t + \left(k_{d_1} + k_{d_2} + \cdots + k_{d_n} \right) \right] \\ f_{d_2} &= x_2 \left[k_t + \left(k_{d_2} + \cdots + k_{d_n} \right) \right] + k_{d_1} x_1 \\ &\vdots \\ f_{d_n} &= x_n k_t + \textstyle\sum_{j=1}^{n} k_{d_j} x_j \end{aligned} \tag{7}$$

The following relationship can be deduced by analogy:

$$f_{d_{j+1}} - f_{d_j} = \left(x_{j+1} - x_j \right) \left(k_t + \sum_{i=j+1}^{n} k_{d_i} \right) \tag{8}$$

Based on the given data set, the interpolation polynomial in the Lagrange form [44] is defined by:

$$L(x) \coloneqq \sum_{j=0}^{k} f_{dj} l_j(x) \tag{9}$$

$$l_j(x) \coloneqq \prod_{\substack{0 \le i \le k \\ i \ne j}} \frac{x - x_i}{x_j - x_i} = \frac{(x - x_0)}{(x_j - x_0)} \cdots \frac{(x - x_{j-1})}{(x_j - x_{j-1})} \frac{(x - x_{j+1})}{(x_j - x_{j+1})} \cdots \frac{(x - x_k)}{(x_j - x_k)} \tag{10}$$

The dry friction force can also be approximated by an interpolation function of physical displacement coordinates. Its hysteresis loop is deduced afterwards by Masing's rule - referred to as the "generalized Masing model". The friction model is obtained by curve fitting based on the least squares method with experimental data. The polynomial coefficients are determined by physical based constraints. Features such as the capability to replicate friction, the Stribeck effect and pre-sliding displacement can all be taken into account by selecting proper polynomial coefficients for the friction formulation. Here the dry friction law is approximated by a polynomial function, where a_1 is determined by the initial slope (the complete stick state), a_2 represents the curvature of the loading curve, a_3 and a_4 are calculated with the static stiffness and the threshold of the dry friction elements (threshold of slip state). The damping force is written by Eq. (11) and the corresponding first loading curve is a smooth curve as shown in Fig. 4.

$$f = \begin{cases} P(x) = a_1 x + a_2 x^3 + a_3 x^5 + a_4 x^7 & x \in [0, x_p] \\ P(x_p) + k_t (x - x_p) & x \in [x_p, +\infty] \end{cases} \tag{11}$$

3. Theoretical aspects of the reduced nonlinear modal analysis using generalized Masing model

The modal synthesis method, which provides numerical efficiency in calculating the steady state responses of complex structures, is presented in the following. The governing equation of a discrete nonlinear model reads:

$$\mathbf{M}\ddot{\mathbf{u}} + \mathbf{D}\dot{\mathbf{u}} + \mathbf{K}\mathbf{u} + \mathbf{f}_{nl}(\mathbf{u}, \dot{\mathbf{u}}) = \mathbf{F}\cos(\omega t) \tag{12}$$

where $\mathbf{u}$ is the vector of the unknown physical displacements, $\mathbf{M}$ is the mass matrix, $\mathbf{D}$ the damping matrix, $\mathbf{K}$ the stiffness matrix, and $\mathbf{F}$ is the amplitude of the harmonic force applied to the system, with ω being the excitation angular frequency. $\mathbf{f}_{nl}(\mathbf{u}, \dot{\mathbf{u}})$ is the nonlinear friction force which depends on the unknown physical displacement and velocity. It can be split into two terms: one a dissipative term depending on the kinetic stiffness k_d and the other a spring term related to k_t. The first term shows the damping capacity, and the second term implies the shifting of the spring term.

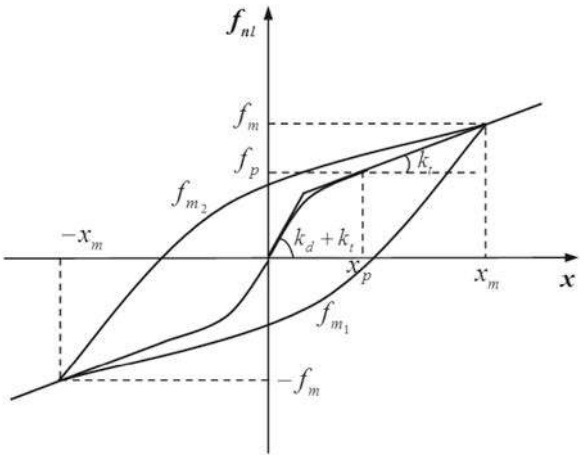

Fig. 4. The hysteresis loop of an infinity of dampers in parallel.

3.1. Strategy guiding the reduced nonlinear modal synthesis based on branch modes

The systems under consideration are large assembled structures and the assumption is that frictional force does not stimulate mode shift. The analysis below is based on the full order FE model containing all the dofs of the system. The determination of the nonlinear normal mode requires iterative procedures. Fewer variables involved in the iterations would lead to a significant savings in computational resources. Component modal synthesis can be applied to project physical coordinates onto the generalized modal coordinates prior to the calculation of nonlinear modes. The double modal analysis based on branch modes may be especially useful for analyzing large assembled systems, since the dofs on the interfaces represent the majority of the dofs and can provide considerable savings in computation time.

The nodes are partitioned into master dofs and slave dofs to facilitate the numerical protocol in **u**, **M**, **K**, **D** and **F**. Master dofs are those on the interface containing frictional nonlinearities that are conserved as physical dofs, while slave dofs are those in the linear substructures. In the following analysis, *S* represents the interior parts of the structure and *J* the junction between substructures. The numbers of master dofs and slave dofs are denoted N_J and N_S, respectively.

The first layer reduction lies in selecting the primary internal modes (free vibration modes of the substructure clamped at its interface) and all the constraint modes (also called static response modes) [45]. All the N_J master dofs are conserved, that is to say, all the constraint modes are conserved. However, the slave dofs are truncated from N_S to N_{S_r}, with $N_{S_r} < N_S$, that is to say, the first N_{S_r} internal modes are selected. The physical displacements of slave dofs are expressed as the addition of a static constraint modes matrix $\mathbf{\Psi}_{SJ}$ multiplied by the physical coordinates of master dofs $\mathbf{u}_J$, plus a reduced internal modes matrix $\mathbf{\Phi}_{SS}$ multiplied by the modal coordinates of the slave dofs $\mathbf{q}_S$:

$$\begin{cases} \mathbf{u}_J = \mathbf{u}_J \\ \mathbf{u}_S = \mathbf{\Psi}_{SJ}\mathbf{u}_J + \mathbf{\Phi}_{SS}\mathbf{q}_S \end{cases} \tag{13}$$

with the static constraint modes $\mathbf{\Psi}_{SJ}$ given by:

$$\mathbf{\Psi}_{SJ} = -\mathbf{K}_{SS}^{-1}\mathbf{K}_{SJ} \tag{14}$$

and the internal modes matrix $\mathbf{\Phi}_{SS}$ formed by eigenvectors $\mathbf{\Phi}_{Sj}$ in the following equation:

$$\left(-\omega_{Sj}^2\mathbf{M}_{SS} + \mathbf{K}_{SS}\right)\mathbf{\Phi}_{Sj} = \mathbf{0} \tag{15}$$

The first layer reduction leads to the internal modes condensation by projecting internal dofs displacements in the physical space onto the modal space, while the number of boundary modes remains the same as that of the boundary dofs. By applying branch modal synthesis, a second reduction is applied to the boundary modes; the boundary dofs displacements $\mathbf{u}_J$ involving frictional nonlinearities are projected onto the modal space by condensing N_J boundary modes onto the N_{J_r} branch modes. ($N_{J_r} < N_J$). The branch modes are the solution of the global structure eigenvalue problem projected onto the constraint modes ($\mathbf{T}_C$). The branch modes matrix $\mathbf{X}_B$ is formed by eigenvectors $\mathbf{X}_{Bj}$ in the following equation [40]:

$$\left(-\omega_{\mathrm{Bj}}^2\mathbf{M}_{\mathrm{B}}+\mathbf{K}_{\mathrm{B}}\right)\mathbf{X}_{\mathrm{Bj}}=\mathbf{0} \tag{16}$$

where

$$\mathbf{M}_{\mathrm{B}}=\left(\mathbf{T}_{\mathrm{C}}\right)^T\mathbf{M}\mathbf{T}_{\mathrm{C}},\quad \mathbf{K}_{\mathrm{B}}=\left(\mathbf{T}_{\mathrm{C}}\right)^T\mathbf{K}\mathbf{T}_{\mathrm{C}},\quad \mathbf{T}_{\mathrm{C}}=\begin{bmatrix}\mathbf{I}_{\mathrm{JJ}}\\ \boldsymbol{\Psi}_{\mathrm{SJ}}\end{bmatrix}$$

After the second reduction, the physical displacements of the system are expressed as follows:

$$\begin{cases}\mathbf{u}_{\mathrm{J}}=\mathbf{X}_{\mathrm{B}}\mathbf{q}_{\mathrm{J}}\\ \mathbf{u}_{\mathrm{S}}=\boldsymbol{\Psi}_{\mathrm{SJ}}\mathbf{X}_{\mathrm{B}}\mathbf{q}_{\mathrm{J}}+\boldsymbol{\Phi}_{\mathrm{SS}}\mathbf{q}_{\mathrm{S}}\end{cases} \tag{17}$$

In matrix form, we have:

$$\mathbf{u}=\begin{bmatrix}\mathbf{u}_{\mathrm{J}}\\ \mathbf{u}_{\mathrm{S}}\end{bmatrix}=\mathbf{T}_{\mathrm{BI}}\begin{bmatrix}\mathbf{q}_{\mathrm{J}}\\ \mathbf{q}_{\mathrm{S}}\end{bmatrix}=\begin{bmatrix}\mathbf{X}_{\mathrm{B}} & \mathbf{0}\\ \boldsymbol{\Psi}_{\mathrm{SJ}}\mathbf{X}_{\mathrm{B}} & \boldsymbol{\Phi}_{\mathrm{SS}}\end{bmatrix}\begin{bmatrix}\mathbf{q}_{\mathrm{J}}\\ \mathbf{q}_{\mathrm{S}}\end{bmatrix} \tag{18}$$

Other component modal synthesis can also be applied to avoid the considerable computational cost. An unavoidable consequence of applying the reduction technique is lower calculation precision. A compromise should thus be made between the accuracy of the reduced model and the computation time according to the client's requirements. A sensitivity analysis of the forced response to $N_{\mathrm{S_r}}$ and $N_{\mathrm{J_r}}$ was described in Ref. [31]. The transformation matrix is denoted $\mathbf{T}_{\mathrm{r}}$ for the generalization for all types of reduction techniques, which project the physical displacements of the system onto the modal coordinates:

$$\mathbf{u}=\mathbf{T}_{\mathrm{r}}\mathbf{q}_{\mathrm{r}} \tag{19}$$

The reduced motion equation is written as:

$$\left(-\tilde{\omega}_{\mathrm{r}}^2\mathbf{M}_{\mathrm{r}}+i\mathbf{D}_{\mathrm{r}}+\mathbf{K}_{\mathrm{r}}\right)\mathbf{q}_{\mathrm{r}}+\left(\mathbf{T}_{\mathrm{r}}\right)^T\tilde{\mathbf{f}}\left(\mathbf{T}_{\mathrm{r}}\mathbf{q}_{\mathrm{r}}\right)=\mathbf{0} \tag{20}$$

$\tilde{\mathbf{f}}\left(\mathbf{T}_{\mathrm{r}}\mathbf{q}_{\mathrm{r}}\right)$ is the modal form of $\mathbf{f}_{nl}\left(\mathbf{u},\dot{\mathbf{u}}\right)$ by using Eq. (19). $\mathbf{M}_{\mathrm{r}}$, $\mathbf{D}_{\mathrm{r}}$ and $\mathbf{K}_{\mathrm{r}}$ are the reduced mass matrix, damping matrix, stiffness matrix:

$$\mathbf{M}_{\mathrm{r}}=\left(\mathbf{T}_{\mathrm{r}}\right)^T\mathbf{M}\mathbf{T}_{\mathrm{r}},\quad \mathbf{D}_{\mathrm{r}}=\left(\mathbf{T}_{\mathrm{r}}\right)^T\mathbf{D}\mathbf{T}_{\mathrm{r}},\quad \mathbf{K}_{\mathrm{r}}=\left(\mathbf{T}_{\mathrm{r}}\right)^T\mathbf{K}\mathbf{T}_{\mathrm{r}} \tag{21}$$

3.2. Theory of nonlinear modal synthesis

In general, the slip on the interface is a result of dynamic magnification around the resonances. It is therefore justifiable to represent the response around the resonance by one single nonlinear mode, which corresponds to the stationary solution in resonant condition [32]:

$$\mathbf{u}_j\approx q_j\tilde{\boldsymbol{\Phi}}_j\left(q_j\right) \tag{22}$$

where $\mathbf{u}_j$ is the displacement induced by one single nonlinear mode-*j*; q_j is the modal amplitude of mode-*j*, $\tilde{\boldsymbol{\Phi}}_j$ is the nonlinear mode shape-*j*. For a full order model, the nonlinear mode $\left(\tilde{\omega}_{\mathrm{j}},\tilde{\boldsymbol{\Phi}}_{\mathrm{j}}\right)$ with $(1+N_{\mathrm{J}}+N_{\mathrm{S}})$ unknowns is included in the nonlinear problem.

Regarding the reduced model using component modal synthesis, the single mode response is given by:

$$\mathbf{u}_j\approx q_j\mathbf{T}_{\mathrm{r}}\tilde{\boldsymbol{\Phi}}_{\mathrm{rj}}\left(q_j\right) \tag{23}$$

where $\left(\tilde{\omega}_{\mathrm{rj}},\tilde{\boldsymbol{\Phi}}_{\mathrm{rj}}\right)$ is the reduced nonlinear mode, with $1+N_{\mathrm{J_r}}+N_{\mathrm{S_r}}$ variables involved in the nonlinear problem. This would provide a considerable time saving compared with the full order model when applying the numerical iterative procedure to solve the nonlinear problem. For the sake of simplicity, the *r* subscript is not denoted in the following analysis.

The steady state response of the nonlinear system can be expressed as a superposition of selected single nonlinear modes responses (24), which will be clarified later.

$$\mathbf{u}\cos(\omega t) \approx \sum_{j=1}^{N} \mathbf{u}_j \cos(\omega t) \approx \sum_{j=1}^{N_r} q_j \widetilde{\mathbf{\Phi}}_j \cos(\omega t) \tag{24}$$

where $\mathbf{u}$ is the response of the nonlinear system; N is the size of the model; N_r is the number of nonlinear modes pertaining to the approximation of the system response.

Nonlinear modal synthesis entails decoupling Eq. (12) into uncoupled equations using the NNMs concept, and thus reduces the order of the nonlinear problem to be solved. The first loading curve permits obtaining the first harmonic component of frictional force, which is then integrated in the modal synthesis approach. Since the nonlinear force depends on the displacement, a relationship can be established intuitively between the nonlinear mode and the modal amplitude. By implementing the equivalent linearization method, the nonlinear normal modes are determined via iterative methods using an equivalent modal damping factor and an equivalent modal stiffness term for each modal amplitude. The dependence of the nonlinear mode on its corresponding modal amplitude can be obtained by progressively increasing the modal amplitude. For the sake of simplicity, the dependence on q_j is neither denoted herein nor in the following.

By inserting the expression of $\mathbf{u}_j$ in Eq. (12) into the equation of motion, the single nonlinear mode becomes the eigen solution to the following free vibration problem:

$$\left[\left(-\widetilde{\omega}_j^2\mathbf{M} + \mathbf{K}\right)\left(q_j\widetilde{\mathbf{\Phi}}_j\right) + \widetilde{\mathbf{f}}\left(q_j\widetilde{\mathbf{\Phi}}_j\right)\right] = \mathbf{0} \tag{25}$$

To obtain the unknown parameters of the nonlinear mode, Kryloff and Bogoliubov's equivalent linearization method [46] is employed. The key point of this method lies in approaching the nonlinear differential equation with an equivalent linear equation:

$$\left[\left(-\widetilde{\omega}_j^2\mathbf{M} + \widetilde{\mathbf{K}}\right)\left(q_j\widetilde{\mathbf{\Phi}}_j\right)\right] = \mathbf{0} \tag{26}$$

The unknown parameters ($\widetilde{\omega}_j$, $\widetilde{\mathbf{\Phi}}_j$) are solved by minimizing the residue between the equivalent linear model and the nonlinear model, which is expressed as:

$$\varepsilon\left(q_j\right) = \left[\left(-\widetilde{\omega}_j^2\mathbf{M} + \widetilde{\mathbf{K}}\right)\left(q_j\widetilde{\mathbf{\Phi}}_j\right)\right] - \left[\left(-\widetilde{\omega}_j^2\mathbf{M} + \mathbf{K}\right)\left(q_j\widetilde{\mathbf{\Phi}}_j\right) + \widetilde{\mathbf{f}}\left(q_j\widetilde{\mathbf{\Phi}}_j\right)\right] \tag{27}$$

Due to the fact that nonlinear restoring force $\widetilde{\mathbf{f}}\left(q_j\widetilde{\mathbf{\Phi}}_j\right)$ is integrated in the motion equation, both the natural frequencies $\widetilde{\omega}_j$ and the modal shapes $\widetilde{\mathbf{\Phi}}_j$ depend on the modal amplitude q_j. The nonlinear problem is solved by using the Newton-Raphson method according to the steps outlined below: the unknowns of the equation are ($\widetilde{\omega}_j$, $\widetilde{\mathbf{\Phi}}_j$); when the dry friction node is clamped the linear modes (ω_j, $\mathbf{\Phi}_j$) of the system are set as initial conditions for the nonlinear problem corresponding to q_j^0; the dimension of the model is assumed to be N, $N + 1$ variables (1 eigenvalue and N eigenvector components) are involved in the numerical approach. To solve the nonlinear problem, a normalization condition with respect to the mass matrix is imposed:

$$\left(\widetilde{\mathbf{\Phi}}_j\right)^T\mathbf{M}\widetilde{\mathbf{\Phi}}_j = 1 \tag{28}$$

Nonlinear perturbation effects have been integrated in nonlinear natural frequency and nonlinear modes, resulting in a nonlinear stiffness matrix:

$$\widetilde{\lambda}_j = \left(\widetilde{\mathbf{\Phi}}_j\right)^T\widetilde{\mathbf{K}}\widetilde{\mathbf{\Phi}}_j \tag{29}$$

with

$$\left(\widetilde{\mathbf{\Phi}}_j\right)^T\widetilde{\mathbf{K}}\widetilde{\mathbf{\Phi}}_j q_j = \left(\widetilde{\mathbf{\Phi}}_j\right)^T\mathbf{K}\widetilde{\mathbf{\Phi}}_j q_j + \left(\widetilde{\mathbf{\Phi}}_j\right)^T\widetilde{\mathbf{f}}\left(q_j\widetilde{\mathbf{\Phi}}_j\right) \tag{30}$$

Once the nonlinear normal mode $\widetilde{\mathbf{\Phi}}_j$ is obtained, it can be written as a linear combination of linear modes to simplify the utilization of modal parameters. The idea is to represent the nonlinear mode by N_l associated linear modes.

$$\widetilde{\mathbf{\Phi}}_j = \sum_{k=1}^{N_l}\widetilde{\beta}_{jk}\mathbf{\Phi}_k \tag{31}$$

where $\widetilde{\beta}_{jk}$ denotes the participation of the linear normal mode $\mathbf{\Phi}_k$ in the nonlinear mode $\widetilde{\mathbf{\Phi}}_j$ and is given by:

$$\widetilde{\beta}_{jk} = \left(\boldsymbol{\Phi}_k\right)^T \mathbf{M}\widetilde{\boldsymbol{\Phi}}_j \quad (j \neq k) \tag{32}$$

The following relation is thus obtained since the linear modes satisfy the orthogonal property with respect to the mass matrix.

$$\widetilde{\beta}_{jj} = 1 \tag{33}$$

Rather than confining all the components of nonlinear mode shapes, we propose to conserve the participation coefficients $\widetilde{\beta}_{jk}$ as a function of modal amplitude q_j in the following.

Assuming that the damping matrix is proportional to the mass and stiffness matrices of the structure, then Basile's hypothesis can be applied. The structural modal damping is given by:

$$\widetilde{d}_j = \left(\widetilde{\boldsymbol{\Phi}}_j\right)^T \mathbf{D}\widetilde{\boldsymbol{\Phi}}_j \tag{34}$$

3.3. Computation of frictional damping ratio

Two modal synthesis methods can be used to study the dynamic behavior of the system, *i.e.*, by employing either real modes or complex modes. The main difference between these two methods lies in the determination of frictional damping term. Furthermore, by analyzing the nonlinear modal parameters, these two approaches provide a description of the frictional damping phenomena from a modal point of view.

3.3.1. Nonlinear modal synthesis with real modes

When applying real modal synthesis, the dissipative anti-phase component of the friction force corresponding to the dissipative effect is neglected, while the in-phase effect of the friction force corresponding to the tuning absorber is considered. The former is determined afterwards by calculating the ratio between the dissipated energy by the slip and the maximum elastic energy E_m per cycle [47]:

$$\widetilde{\eta}_j = \frac{dE}{E_m} \tag{35}$$

The relationship between the friction force f_{nl} and damper motion x in steady state is governed by the first loading curve. Based on the hysteresis loop, we can obtain the dissipated energy per cycle:

$$dE = \sum_{i=2}^{N_t} \frac{1}{2} \left[f_{nl}(i) + f_{nl}(i-1)\right] \left[x(i) - x(i-1)\right] \tag{36}$$

The maximum displacement in the hysteresis loop is determined by:

$$x_m = \left| q_j \widetilde{\boldsymbol{\Phi}}_j \right| \tag{37}$$

The maximum elastic energy is thus:

$$E_m = \frac{1}{2} \widetilde{\lambda}_j q_j^2 \quad \text{with} \quad \widetilde{\lambda}_j = \widetilde{\omega}_j^2 \tag{38}$$

3.3.2. Nonlinear modal synthesis with complex modes

When employing the complex modal analysis, the eigenvalue and eigenvector are both in complex form, which are expressed as:

$$\widetilde{\lambda}_j = \widetilde{\lambda}_j^c + i\widetilde{\lambda}_j^s \tag{39}$$

$$\widetilde{\boldsymbol{\Phi}}_j = \widetilde{\boldsymbol{\Phi}}_j^c + i\widetilde{\boldsymbol{\Phi}}_j^s \tag{40}$$

Herein f_{nl} is divided into two parts: the imaginary part showing the damping capacity, and the real part implying the shifting of the spring term:

$$\mathbf{f}_{nl} = \mathbf{f}_{nl}^c + i\mathbf{f}_{nl}^s \tag{41}$$

The real part and imaginary part of the dry friction force are deduced by retaining the first harmonic component of the nonlinear force when transforming the first loading curve from the time domain to the frequency domain. This procedure has highlighted the role of the first loading curve described in Section 2. The corresponding frictional damping factor is no longer obtained by calculating the energy dissipation, while it is directly involved in the deduction of the eigen solutions in Equation (20). Using the complex modal formulation, the frictional damping factor is determined directly by the ratio between $\widetilde{\lambda}_j^s$ and $\widetilde{\lambda}_j^c$.

$$\widetilde{\eta}_j = -\frac{\widetilde{\lambda}_j^s}{\widetilde{\lambda}_j^c} \tag{42}$$

3.4. Calculation of the steady state response

Another advantage of this method is that nonlinear normal modes can be computed once and then used for calculating all types of external loading. The modal parameters $\widetilde{\omega}_j$, $\widetilde{d}_j$ and $\widetilde{\eta}_j$ are then interpolated with respect to the modal amplitude q_j, and they are independent of excitation loads. When calculating the frequency response with this method, the inversion of the matrices is a simple algebraic division instead of complex inversion of matrix. This may lead to a significant reduction in computation time. When the modes are slightly coupled, the nonlinear forced responses can be obtained by the superposition of forced responses induced by the single nonlinear normal mode. Admittedly, the coupling between the nonlinear modes are not considered by using this approach.

The response of the model subjected to harmonic excitations around the resonant frequency ω_j is approximated by mode - *j*:

$$\left(\widetilde{\mathbf{\Phi}}_j\right)^T \left(-\omega^2\mathbf{M} + i\mathbf{D} + \widetilde{\mathbf{K}}\right)\widetilde{\mathbf{\Phi}}_j q_j = \left(\widetilde{\mathbf{\Phi}}_j\right)^T \mathbf{F} \tag{43}$$

Using the interpolation models of $\widetilde{\omega}_j$, $\widetilde{d}_j$ and $\widetilde{\beta}_{jk}$ with respect to the modal amplitude q_j, the modal amplitude is given by:

$$q_j = \frac{\widetilde{f}_j\left(\left|q_j\right|\right)}{-\omega^2 + i\widetilde{d}_j\left(\left|q_j\right|\right) + \widetilde{\omega}_j^2\left(\left|q_j\right|\right)\left(1 + i\widetilde{\eta}_j\left(\left|q_j\right|\right)\right)} \tag{44}$$

where

$$\widetilde{f}_j\left(\left|q_j\right|\right) = \left(\widetilde{\mathbf{\Phi}}_j\left(\left|q_j\right|\right)\right)^T \mathbf{F} \tag{45}$$

The solution to Eq. (44) is obtained by assuming that the dependence of the nonlinear parameters on q_j in the equation are known. This explains why these modal parameters are interpolated with respect to q_j. The determination of q_j in Eq. (44) turns out to be a scalar nonlinear problem corresponding to the excitation frequency ω. The single nonlinear response $\mathbf{u}_j$ is given by Eq. (22). In the case of a reduced order model, the single nonlinear response of the full order model is obtained by projecting the modal coordinates onto the physical space with the reduction basis $\mathbf{T}_r$ by using Eq. (19). The single normal mode method corresponding to Eq. (24) allows reproducing the response diagram of the model, which is done by superimposing the forced responses $\mathbf{u}_j$ of mode-*j*.

The entire algorithm for computing the nonlinear modes and forced responses of the nonlinear model involving dry friction is illustrated in Fig. 5.

4. Simulation results and discussion

Three case studies are described in this section.

- Firstly, we consider a simple 2-dofs lumped-parameter system. Both the bilinear model and the generalized Masing model are employed to describe the frictional damping device, then the implications of the results in the light of the differences between them are discussed. The forced responses of the system are computed using both real and complex nonlinear modal synthesis approaches. The results are compared to those obtained with HBM and the Newmark-β method for the purpose of validation. A modal overview of the nonlinear behavior of the frictional system is also provided.
- Secondly, a continuous cantilever beam system is investigated. The forced responses and a modal overview, are provided by applying nonlinear modal synthesis approaches.

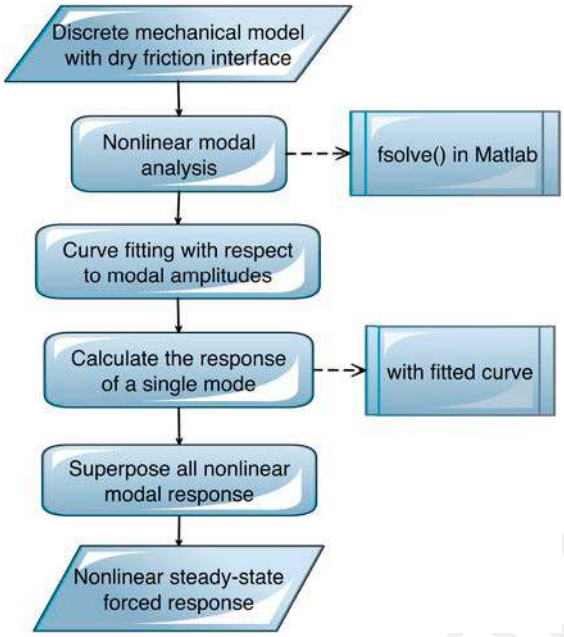

Fig. 5. Algorithm for the computation of forced responses of mechanical model involving dry friction.

- Lastly, we study an assembled system composed of Kirchhoff plates and the frictional damping devices distributed continuously along the interface between substructures. The computational time resulting from the different methods is compared to show the efficiency of the proposed nonlinear modal synthesis approach. Reduction techniques are also applied to obtain a reduced-order model which yields a reduced nonlinear modal synthesis.

4.1. Case study of a 2-dofs mass-stiffness system

The 2-dofs lumped-parameter system is often used to describe and validate strategies, as in Refs. [3,48]. The mass on the left ($m_1 = 1$ kg) is clamped to the wall and the mass on the right ($m_2 = 1$ kg) is attached to the dry friction device, as shown in Fig. 6. The system is excited by a tire balance type loading on m_1: $\mathbf{F} = m\omega^2 R \cos \omega t$ at frequency ω, with $m = 6$ g and $R = 4$ cm. The tire balance loading corresponds to a real case that describes the distribution of mass within an automobile tire to which it is attached. The excitation frequency band investigated is [8, 70] Hz. Friction damping elements are connected to m_2. A slight viscous structural damping is integrated in the model, with a damping ratio of 0.05% proportional to the stiffness matrix ($k_1 = 600$ N/m, $k_2 = 400$ N/m).

When the dry friction damper is modeled by a bilinear model with $k_t = 1/2000 * k_2$, $k_d = 1/20 * k_2$ and $\mu_d = 0.5$, the temporal histories of the displacement and the friction force can be obtained by using the Newmark-β method ($\beta = 0.25$ and $\gamma = 0.5$). For a normal force of 5 N, the time histories of damping point displacement, friction force and displacement-friction curve are shown in Figs. 7, 9 and 11. Their corresponding steady state curves are shown in Figs. 8, 10 and 12. In Figs. 8 and 10, it can be seen that slip occurs when the large amplitude displacement of the damping point takes place. The dissipated energy induced by the slip in one stable period is represented by the enclosed surface shown in Fig. 12. It is noteworthy that numerous periods are needed to obtain the steady state response. A more efficient method is required when emphasis is placed on qualitative trends in the dynamic behavior of the generic system and the steady state forced response.

For a normal load of 35 N, the steady state responses of m_1 and m_2 obtained with real modal synthesis (reported in asterisk marks) and complex modal synthesis (reported in circle marks) are compared with those obtained with the

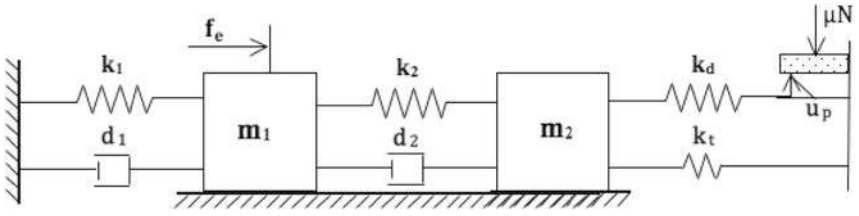

Fig. 6. 2-dofs model with dry friction modeled by one damper.

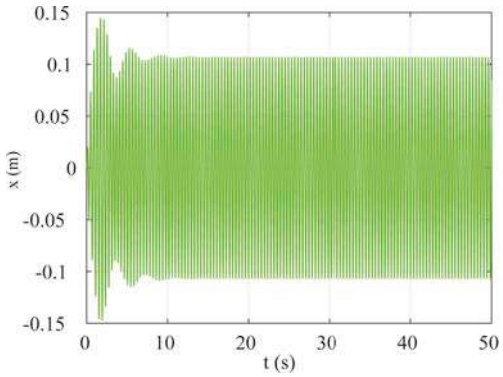

Fig. 7. Time history of m_2 displacement obtained with Newmark-β method.

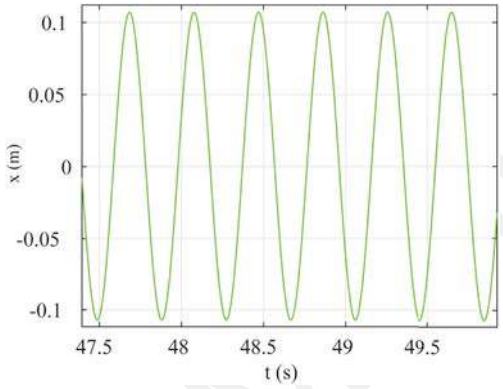

Fig. 8. Steady state displacement of m_2 obtained with Newmark-β method.

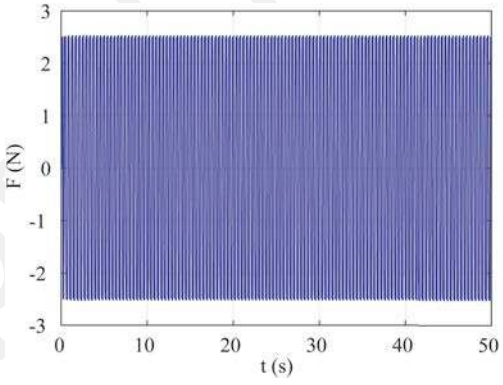

Fig. 9. Time history of friction force obtained with Newmark-β method.

Newmark-β method (reported in plus marks) and the HBM method (marked in solid line), as depicted in Fig. 13 for m_1 and Fig. 14 for m_2. These figures show response curves that closely match the reference, revealing that the nonlinear modal synthesis method is efficient in calculating the forced response without sacrificing accuracy, especially if we consider the complexity of the nonlinear effect being synthesized.

The influence of normal loads on the dynamic performance of the system is also analyzed. The steady state responses of m_1 and m_2 corresponding to eight normal loads - 0, 15, 20, 25, 85, 150, 200 and 8000 N (denoted *Inf* in the figures) - are plotted in Figs. 15 and 16 by using complex modal synthesis. As can be seen, the variation of normal load affects the resonant peak level and resonant frequency value. All these figures reveal the damping effect around the resonance and the damper tuning effect of the friction device. The resonant frequency is dislocated or, more specifically, becomes larger when the normal force increases. In the meantime, the damping level varies with the normal load level. The optimal normal load allowing maximal frictional damping in the neighborhood of the first resonance is around 20 N for both m_1 and m_2; the optimal normal load that allows a maximal frictional damping in the neighborhood of the second resonance is around 150 N for both m_1 and m_2, as shown in Figs. 15 and 16.

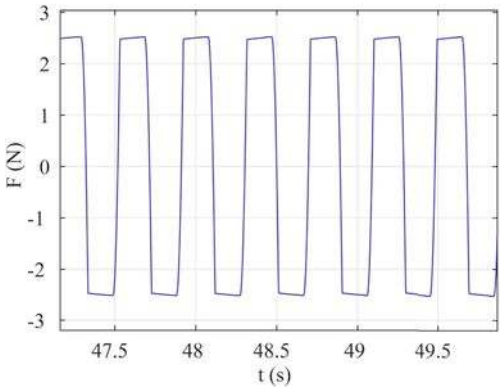

Fig. 10. Steady state friction force obtained with Newmark-β method.

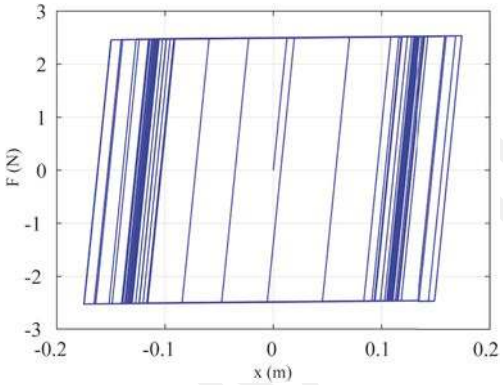

Fig. 11. Time history of friction force in function of m_2 displacement obtained with Newmark-β method when the normal load equals to 5 N.

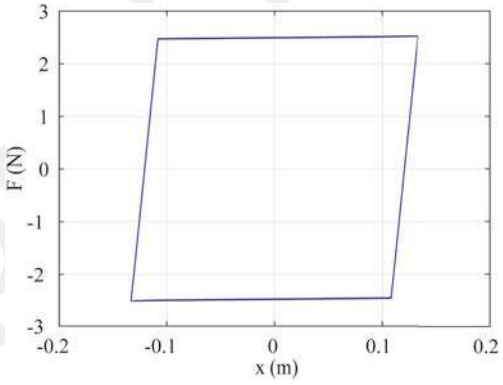

Fig. 12. Steady state first loading curve obtained with Newmark-β method when the normal load equals to 5 N.

Further insight into the qualitative nature of the dynamic response can be obtained by analyzing the equivalent natural frequency and modal damping ratio. Figs. 17 and 18 present the variation of natural frequency and frictional modal damping factor with respect to the modal amplitude for these two modes, corresponding to different normal load values. It can also be seen that nonlinear natural frequencies all stem from the linear natural frequencies of the underlying system with dynamic stiffness and finally approximate the linear natural frequencies of the system without dynamic stiffness, which is also reasonable, since $q = 0$ corresponds to the system in complete slip state and $q \rightarrow + \infty$ corresponds to the system in stick state. The low level modal amplitude corresponds to the case in which the system features a crack, and the high level modal amplitude conforms to the case in which the corresponding nonlinear boundary conditions are ignored. The evolution of the modal damping factor exhibits a maximum, which accounts for an optimum nonlinear damping due to the friction element. It should be noted that the maximal damping value does not depend on the normal load applied on the friction element.

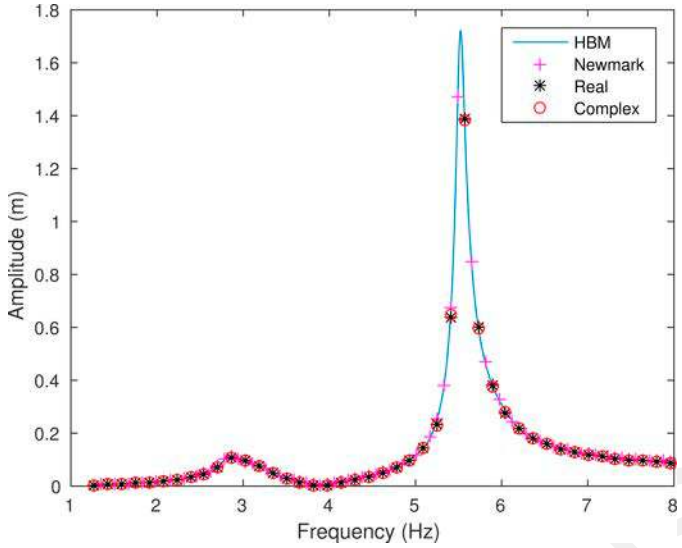

Fig. 13. Comparison of forced response of m_1 obtained with real modal synthesis, complex modal synthesis, HBM and Newmark method.

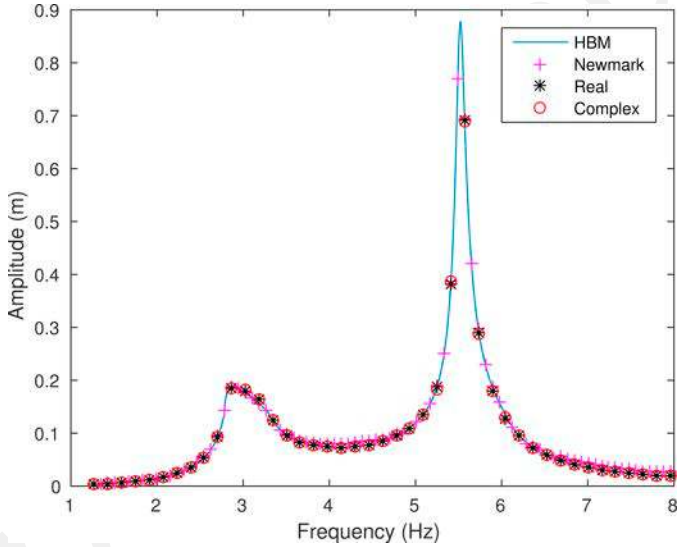

Fig. 14. Comparison of forced response of m_2 obtained with real modal synthesis, complex modal synthesis, HBM and Newmark method.

In the case where the dry friction model is modeled using the generalized Masing model, the variation of modal parameters with respect to the modal amplitude is indicated in Fig. 19 for the first mode and in Fig. 20 for the second mode. If we compare Figs. 17 and 18 with Figs. 19 and 20, the difference between the bilinear Zener model and the generalized Masing model is that the variation of natural frequency and frictional modal damping occurs immediately and continuously when slip takes place for the generalized Masing model. For example, both the modal frequency and the modal damping in Figs. 17 and 18 initiate their variations when modal amplitude attains a certain value, whereas the change of modal frequency and modal damping in Figs. 19 and 20 takes place immediately when the modal amplitude differs from 0.

4.2. Case study of a cantilever beam

Except for the 2-dofs mass stiffness system, simulations were also performed on a continuous cantilever beam. The beam length is 5 m. An external sinusoidal excitation is applied on $x = 2$ m in the opposite direction of y. A Rayleigh type damping is integrated in the structure, with $\alpha = 1$ and $\beta = 3 * 10^{-4}$. The translation in the z direction and rotations around x and y axis are neglected. The left end is clamped to the wall. The right end is simply supported and

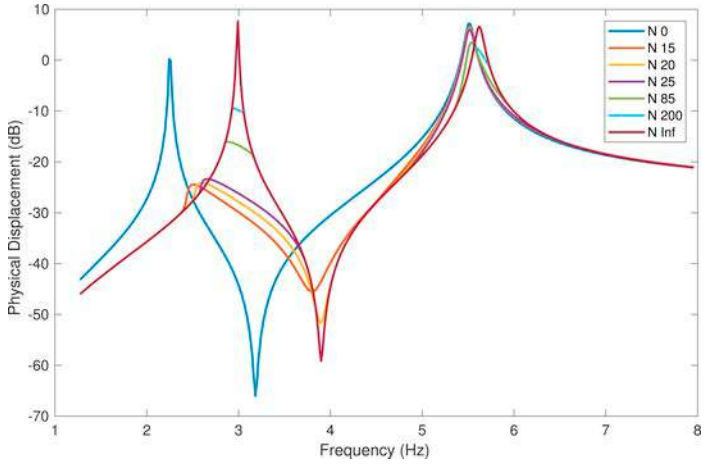

Fig. 15. Forced response of m_1 corresponding to different normal load level of bilinear model. *N* denotes the normal load.

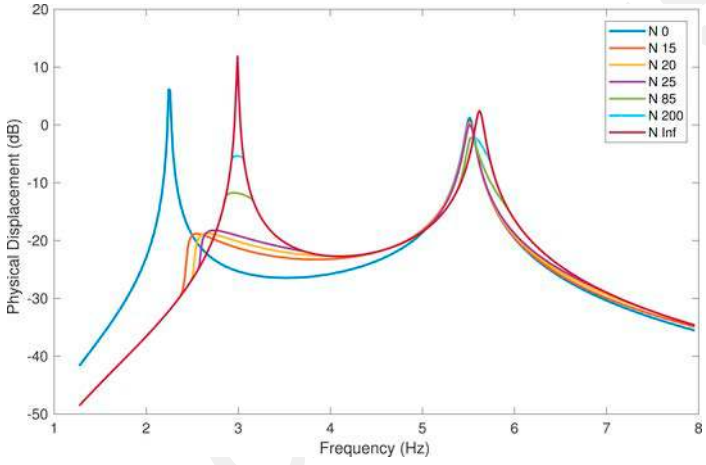

Fig. 16. Forced response of m_2 corresponding to different normal load level of bilinear model. *N* denotes the normal load.

linked to a torsional spring as illustrated in Fig. 21. The movement of the right end in θ_z direction follows the dry friction law of a bilinear Zener model.

Time histories as well as steady state responses can be obtained with the Newmark-β method. For a harmonic excitation with an amplitude of 10 N and a normal load of 10 N applied on the right end, the steady state response, the frictional force and the first loading curve of the node linked to the torsional spring are plotted in Figs. 22–24. In Figs. 22 and 23, it can be seen that both stick and slip states occurred, and that slip state takes place only when the amplitude is large. The enclosed surface in Fig. 24 represents the energy dissipated by the friction force.

Similar to the 2-dofs case, a comparative study of forced responses is conducted by using the Newmark-β method, the HBM method and real and complex nonlinear modal synthesis approaches. The forced responses of the excitation node and friction point in the *y* direction are compared in Figs. 25 and 26. The responses obtained with the HBM method are reported in solid blue lines, those with the Newmark-β method are given in plus marks and those of real modal synthesis are given by black circles. All these figures show that the response curves closely match with each another, thereby validating the nonlinear modal synthesis method for a continuous system.

Since the nonlinear modal synthesis method has been proven efficient, it can be employed to identify the optimal normal load applied on the contact point for an optimal frictional damping. When observing forced responses around the first resonance obtained with modal synthesis methods, the response curves corresponding to different normal loads (5, 10, 18, 25, 30 and 35 N) are plotted in Fig. 27 for the excitation point and Fig. 28 for the frictional point. The optimal normal load, which allows maximal frictional damping in the neighborhood of the first resonance, is around 25 N.

Further insight into the qualitative nature of the dynamic response is gained by examining the equivalent natural frequency and frictional modal damping ratio of the first mode. Fig. 29 presents the variation of the natural frequency

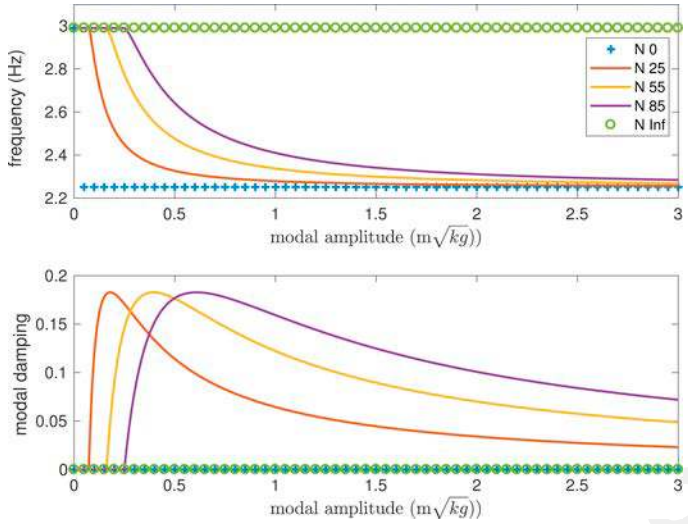

Fig. 17. Evolution of natural frequency and modal damping factor in terms of modal amplitude, corresponding to different normal load level, using bilinear model.

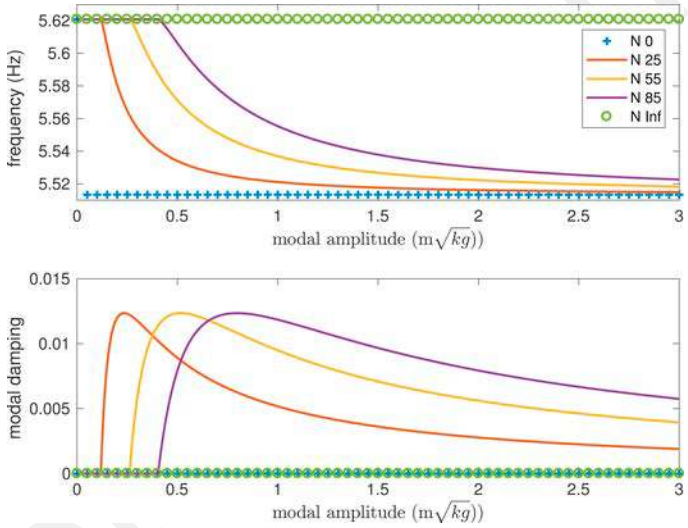

Fig. 18. Evolution of natural frequency and modal damping factor in terms of modal amplitude, corresponding to different normal load level, using bilinear model.

and modal damping factor with respect to the modal amplitude, corresponding to different normal load values on the friction point. The nonlinear natural frequencies all stem from the linear natural frequency of the underlying system with dynamic stiffness (16.3 Hz) and finally approximate the linear natural frequency of the system without the dynamic stiffness (14.7 Hz). The maximum modal damping does not depend on the normal load, *i.e.* when the value of the normal load changes, the value of maximum modal damping (0.065) remains the same. Note that the modal amplitude corresponding to the maximum modal damping varies with the normal load.

4.3. Case study of a plate assembly system

The torsional friction element used in the beam system is then applied to the interface connecting two substructures. The assembled system contains two Kirchhoff plates and one rubber layer interface. Plate 1 on the left side is denoted by S_1, with the length $a_1 = 0.66\,\text{m}$, the width $b_1 = 0.6\,\text{m}$ and the thickness $e = 0.002\,\text{m}$. Plate 2 on the right is denoted by S_2, with the length $a_2 = 0.44\,\text{m}$, the width $b_2 = 0.6\,\text{m}$ and thickness $e = 0.002\,\text{m}$. The rubber material, with the thickness $\theta = 0.002\,\text{m}$ and the width $l = 0.003\,\text{m}$, is padded on both the top and the bottom of the plates so as to ensure the connections between S_1 and S_2. The variation of the thickness and width of the rubber layer affects the change in its stiffness value [40]. The model is excited with a tire balance type loading [49]: $\mathbf{F} = m\omega^2 R\cos\omega t$ at a frequency ω, with $m = 6\,\text{g}$, $R = 4\,\text{cm}$, and the frequency of interest from 0 to 16 Hz. The exci-

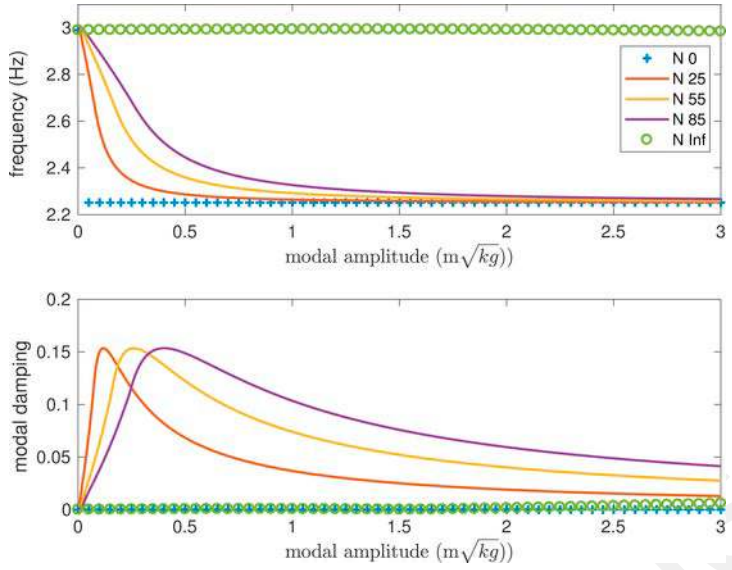

Fig. 19. Evolution of natural frequency and modal damping factor in terms of modal amplitude, corresponding to different normal load level, using generalized Masing model.

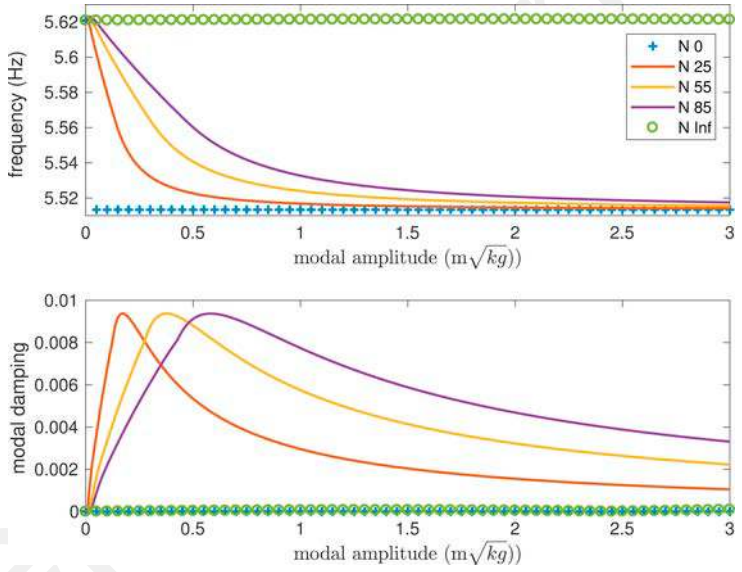

Fig. 20. Evolution of natural frequency and modal damping factor *vs.* modal amplitude, corresponding to different normal load level, using generalized Masing model.

Fig. 21. The cantilever beam model.

tation is located at $x = 0.44\,\mathrm{m}$ and $y = 0.2\,\mathrm{m}$, hence lying on S_1. Dry friction devices are continuously distributed along the interface, acting as torsional forces between S_1 and S_2. The nonlinear frictional forces are assumed to lie in the torsional direction θ_y. The relation between the friction force and the relative displacement between S_1 and S_2 in the θ_y direction obeys the dry friction law of a bilinear Masing model. The dry friction damper is modeled by a bilinear model with $k_d = 50$, $k_t = 1/100 * k_d$ and $\mu_d = 0.5$.

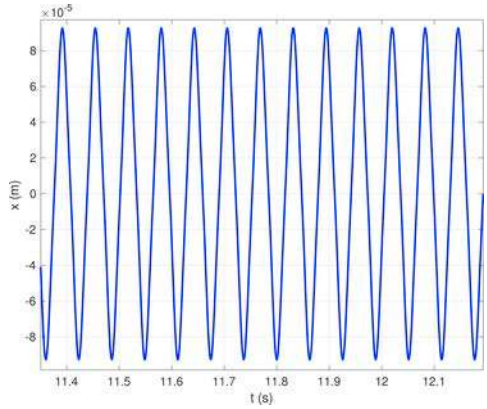

Fig. 22. Stabilized displacement of the right end in y direction obtained with Newmark-β method.

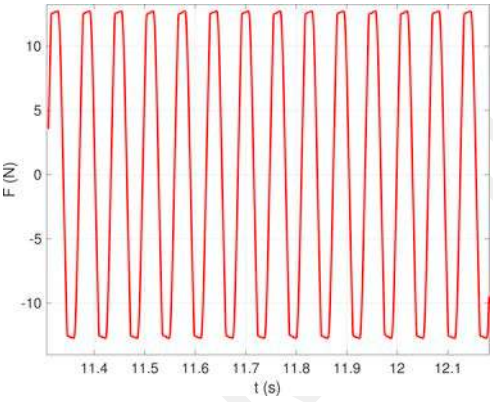

Fig. 23. Stabilized friction force obtained with Newmark-β method.

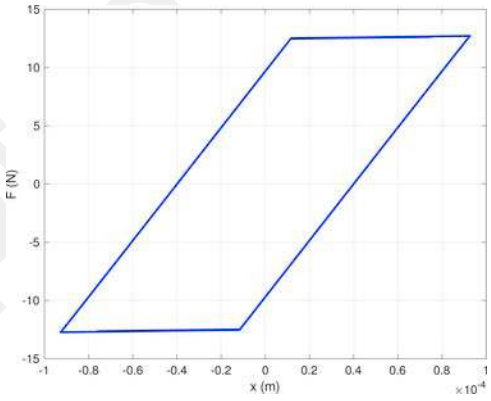

Fig. 24. Stabilized first loading curve obtained with Newmark-β method.

The values of normal force applied on the dry friction contact along the interface are all equal to 0.01 N. A viscous damping has been integrated in the model with a damping ratio of 0.02 directly proportional to the stiffness matrix. The stabilized response of node 1 (see Fig. 30) is plotted in Fig. 31 using Newmark-β method. The steady state figure of the friction force of the torsional spring linked to node 1 is shown in Fig. 32. It can be seen that both stick and slip states occurred. The stabilized displacement-friction force curve is also shown in Fig. 33. The enclosed surface represents the energy dissipated by this friction device in steady state.

A comparative study of forced responses is conducted by using the Newmark-β method, the HBM method with the first three harmonics, the HBM method with the first harmonic, and the nonlinear modal synthesis based on real modes and complex modes. The forced responses of the excitation node in z direction is given in Fig. 34 for an amplitude of external sinusoidal load equal to 0.25 N and the normal loads applied on the friction contacts equal to 0.01 N.

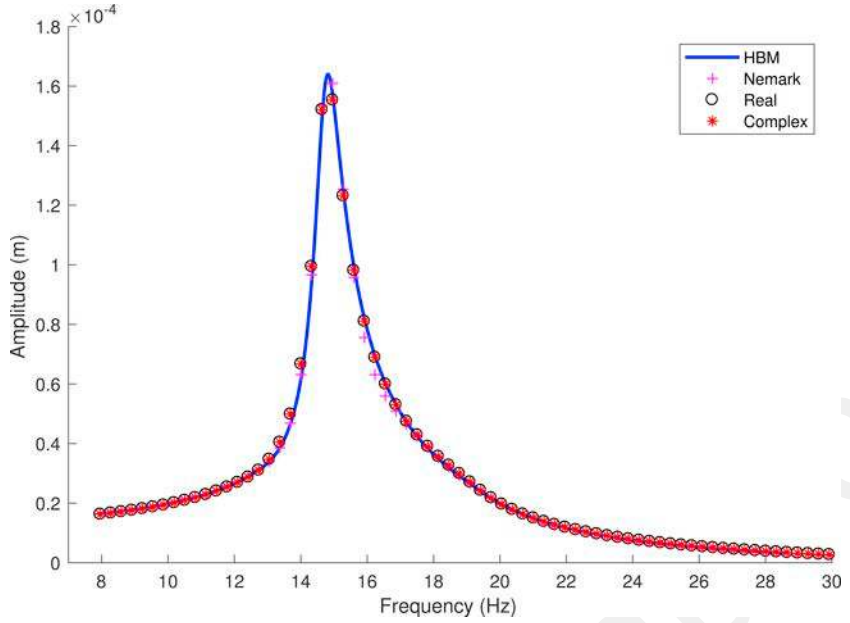

Fig. 25. Comparison of forced response of excitation point obtained with complex modal synthesis, HBM and Newmark method.

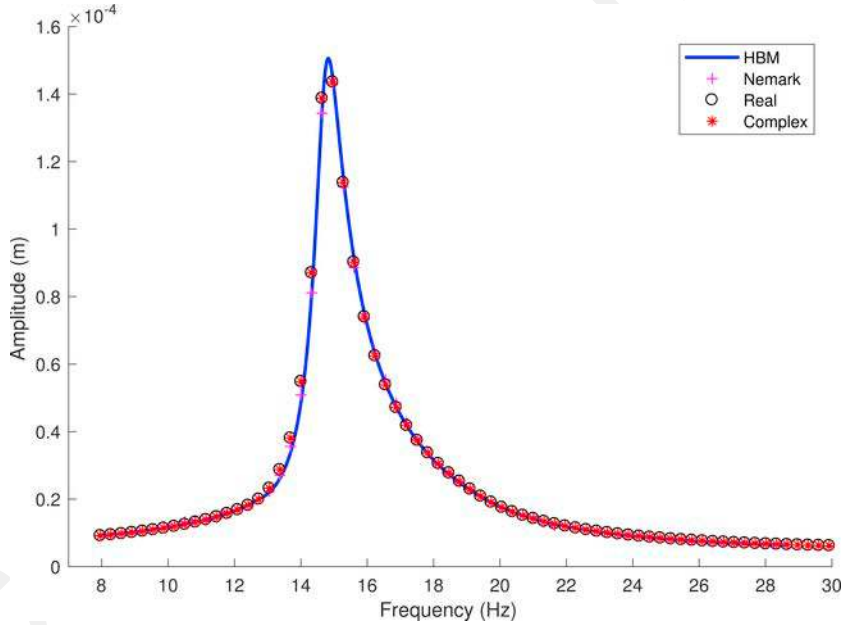

Fig. 26. Comparison of forced response of friction point obtained with complex modal synthesis, HBM and Newmark method.

The response obtained with Newmark-β method is shown in a solid black line, the HBM method with the first three harmonics by a solid blue line, HBM method with the first three harmonics by a solid magenta line, the modal synthesis based on real modes by blue plus marks and the modal synthesis based on complex modes by red asterisk marks. No significant difference is observed between the HBM method with the first three harmonics and that with only the first harmonic. This also justifies the nonlinear modal synthesis by selecting only the first harmonic of frictional force through the use of the first loading curve.

Simulations were run on a server containing 32 Xeon (R) processors operating at 2.9 GHz. Table 1 compares the CPU time consumed to compute the steady state response of the assembled system for a certain frequency using nonlinear modal synthesis, and the HBM and Newmark–β methods. It should be mentioned that the calculation of steady state response is very fast once the relationship between the nonlinear modes and modal amplitudes is established.

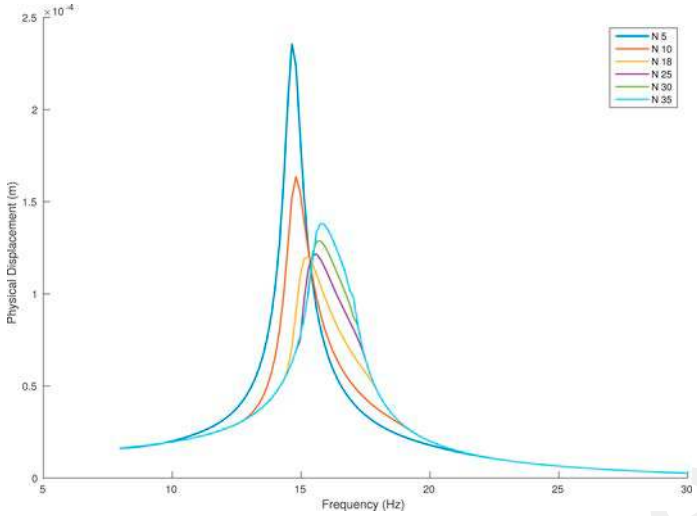

Fig. 27. Forced response in *y* direction of the excitation point corresponding to different normal load level of bilinear model.

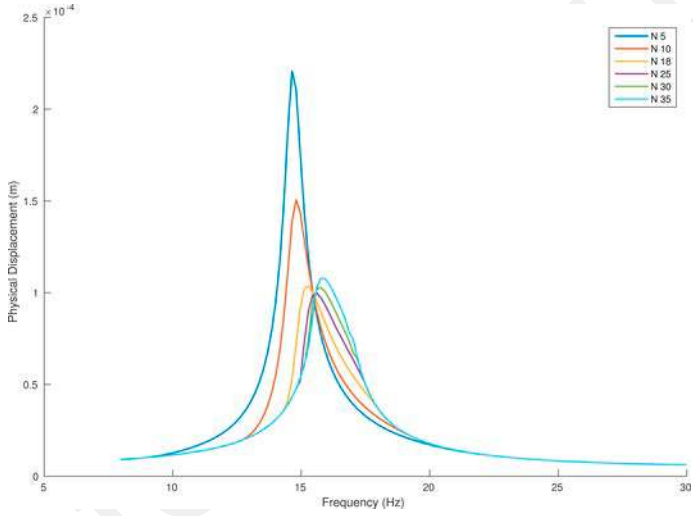

Fig. 28. Forced response in *y* direction of the friction point corresponding to different normal load level of bilinear model.

Otherwise, it takes 6 s to calculate the nonlinear mode corresponding to one modal amplitude, which is also fast. Moreover, it should be noted that the more complex the system is, the more advantageous the method proposed.

Since the nonlinear modal synthesis method has been proven efficient, it can be employed to identify the optimal normal load applied on the contact point for an optimal frictional damping. Response curves corresponding to different normal loads (0, 0.01, 0.02, 0.05, 0.1, 0.3 and 30 N) are plotted in Fig. 35 using the complex modal synthesis method. It should be noted there is no need to increase the normal load when it exceeds 0.3 N, since no significant increase in frictional damping effect is observed when comparing the response curves corresponding to 0.3 and 30 N, which is in accordance with Fig. 36. As shown in Fig. 36, the variation of the natural frequency and frictional damping with respect to modal amplitude for 0.3 N approaches that for 30 N. The optimal normal load, which allows maximal frictional damping in the neighborhood of the first resonance, is around 0.05 N.

Fig. 36 presents the variation of the natural frequency and the modal damping factor with respect to the modal amplitude of the first mode, corresponding to different normal load values on the frictional contacts. The nonlinear natural frequency stems from the linear natural frequency of the underlying system with dynamic stiffness (5.4 Hz) and finally approximates the linear natural frequency of the system without the dynamic stiffness (3.7 Hz). Once again, the maximum modal damping does not depend on the normal load, that is to say, when the value of the normal load changes, the value of the maximum modal damping (0.25) remains the same, which accounts for an optimum nonlinear damping due to the friction element according to Fig. 35.

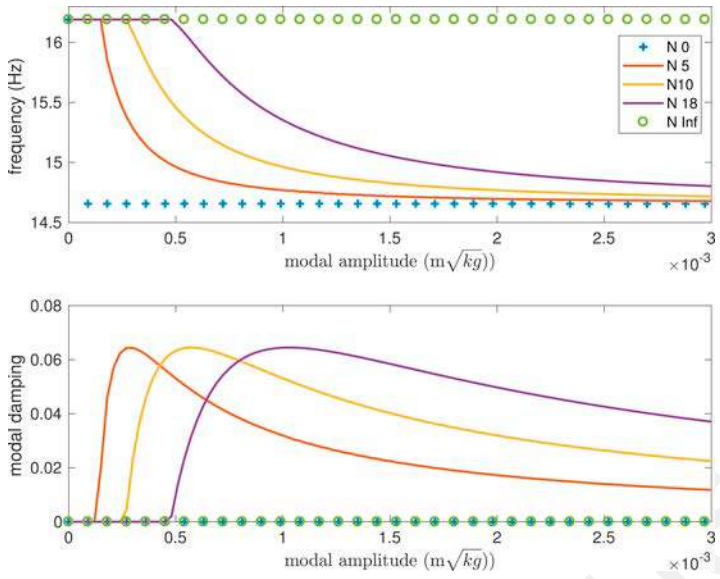

Fig. 29. Evolution of natural frequency and modal damping factor *vs.* modal amplitude, corresponding to different normal load level, using bilinear model.

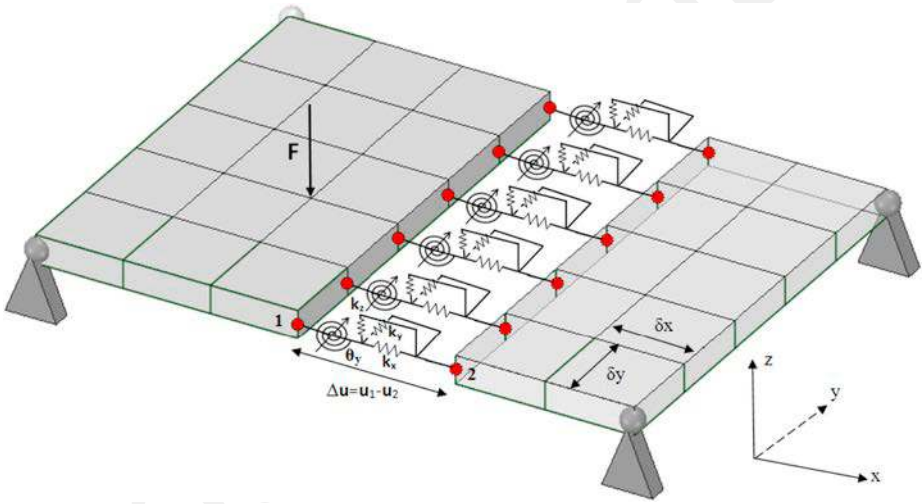

Fig. 30. FE model of the plate.

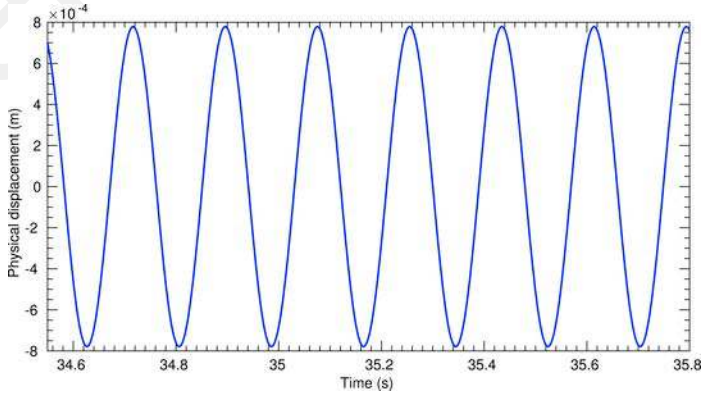

Fig. 31. Stabilized displacement obtained with Newmark-β method.

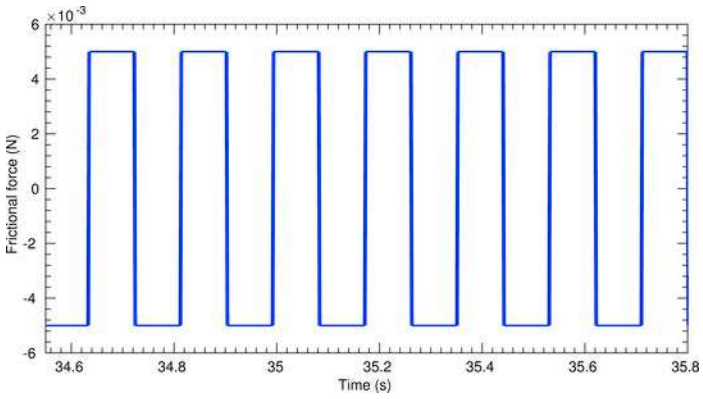

Fig. 32. Stabilized friction force obtained with Newmark-β method.

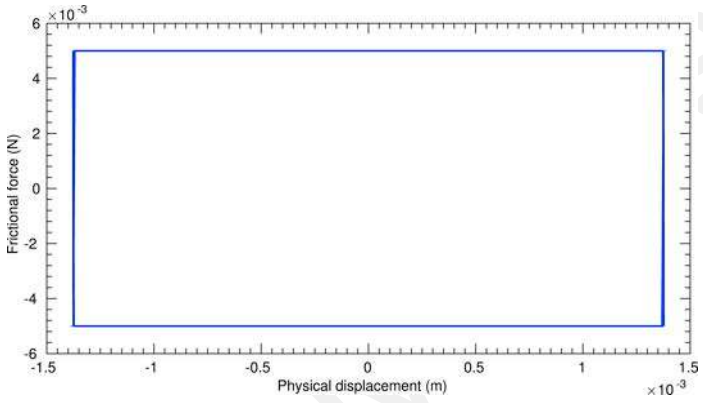

Fig. 33. Stabilized loading curve obtained with Newmark-β method.

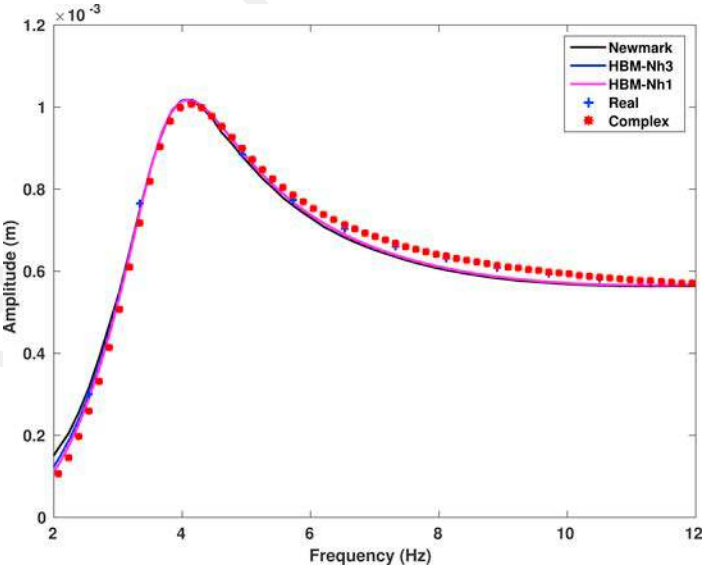

Fig. 34. Comparison of forced response of excitation point obtained with real modal synthesis, complex modal synthesis, HBM-3 harmonics, HBM-1 harmonic and Newmark method.

A similar study can be carried out for other modes of the plate by using nonlinear modal synthesis. We take mode 5 arbitrarily as another example, and structural hysteresis damping with a damping ratio of 0.02 is applied on the model. When observing the forced response curves corresponding to different normal loads (0, 0.05, 0.125, 0.2, 0.25, 0.5 and 20 N) in Fig. 37, the optimal normal load for an optimal frictional damping for mode 5 is found to be around

Table 1
CPU time comparison of different methods to obtain steady state response.

Methods	Newmark–β Method	Harmonic Balance Method	Nonlinear Modal Synthesis
CPU time(s)	44	22	3

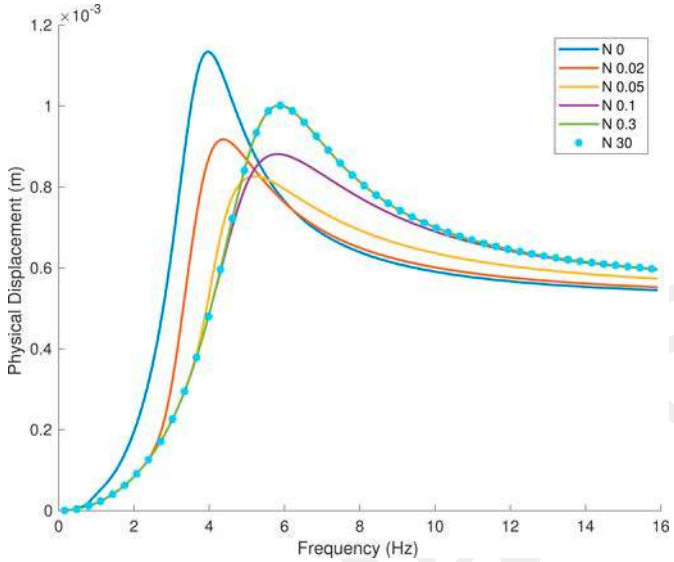

Fig. 35. Forced response of excitation point corresponding to different normal load level of the plate for mode 1. *N* denotes the normal load applied on the dry friction contact.

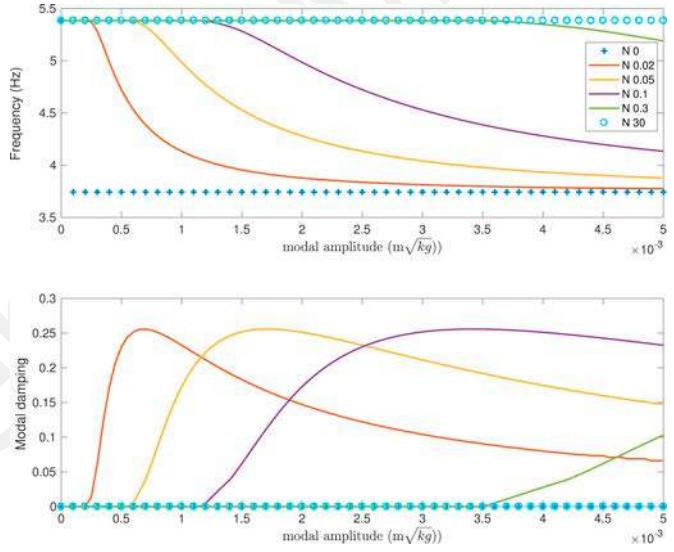

Fig. 36. Evolution of natural frequency and modal damping factor in terms of modal amplitude for mode 1, corresponding to different normal load level, using bilinear model.

0.25 N. Similarly, when the normal load exceeds 2 N, there is no significant difference between the response curves with that of 20 N, as shown in Fig. 37. This phenomenon can be explained by Fig. 38, that is to say, when the modal amplitude varies between 0 and the maximum modal amplitude that the system could attained around this resonance, the natural frequency and frictional modal damping ratio for 2 N are the same as that for 20 N. The variation of the natural frequency and the modal damping factor in terms of modal amplitudes for mode 5 is shown in Fig. 38. The nonlinear natural frequency for mode 5 stems from the linear natural frequency of the underlying system with dynamic stiffness (26.3 Hz) and finally approximates the linear natural frequency of the system without the dynamic

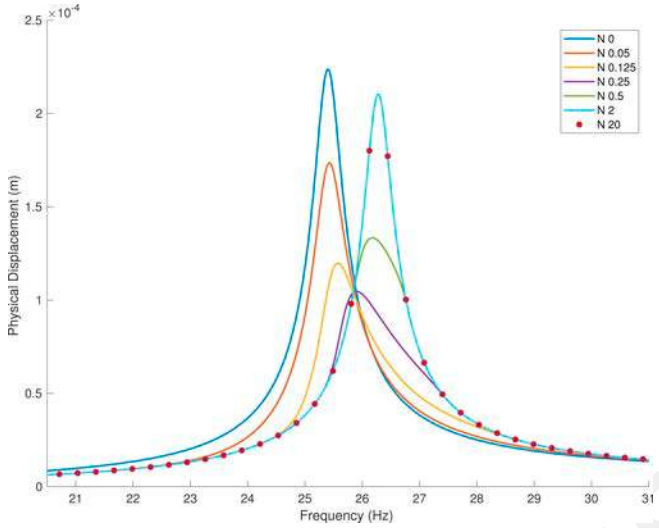

Fig. 37. Forced response of excitation point corresponding to different normal load level of the plate for mode 5. *N* denotes the normal load applied on the dry friction contact.

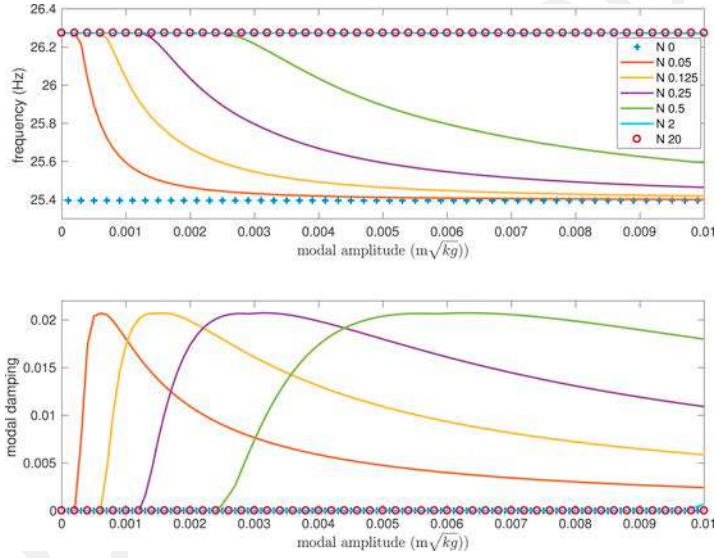

Fig. 38. Evolution of natural frequency and modal damping factor in terms of modal amplitude for mode 5, corresponding to different normal load level, using bilinear model.

stiffness (25.4 Hz). Once again, the maximum modal damping does not depend on the normal load, *i.e.* when the value of the normal load changes, the value of the maximum modal damping (0.02) remains the same, which accounts for an optimum nonlinear damping arising from the friction element according to Fig. 37. These results have also proven the effectiveness of nonlinear modal synthesis in the analysis of a more complicated assembled system with friction devices continuously distributed along the interface.

Moreover, the dimension of the assembled system can be reduced by using branch mode analysis, which economize even more computational resources. All reduction techniques serve to lower computation time. Double modal synthesis is even more advantageous compared to classical one-layer reduction as it also condenses boundary modes. The component modes under 50 Hz are kept to describe the dynamic performance of the system around the first resonance mode. The full FE model contains 168 dofs, while the reduced model consists of 14 modes, *i.e.* 9 branch modes, 1 excitation mode, 3 internal modes of S_1 and 1 internal mode of S_2. By applying the branch modal synthesis method, 92% dofs are cut off and the size of the nonlinear problem is much smaller. The time taken to compute a nonlinear mode for a given modal amplitude is reduced from 1.7 s to 0.3 s (83%), and that for solving the modal amplitude for a given excitation frequency is reduced from 3 s to 1.5 s (50%). The optimal normal load for controlling the first resonant mode is found to be around 0.05 N by employing branch mode analysis, as shown in Fig. 39. This is

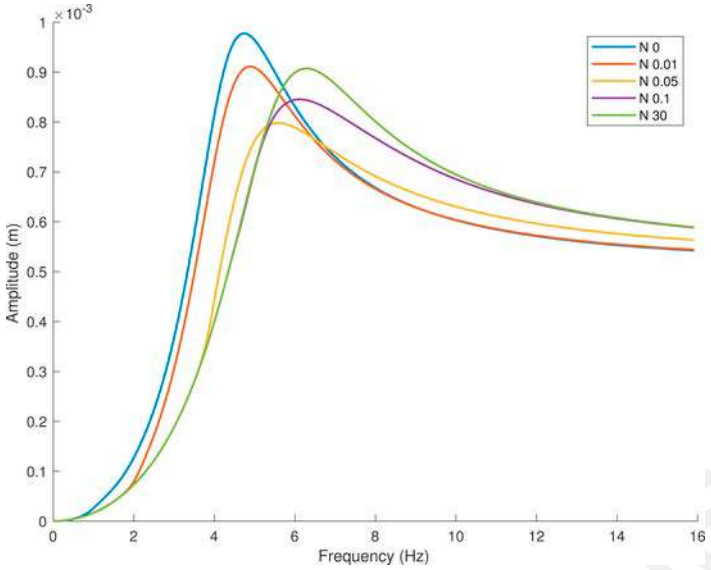

Fig. 39. Forced response of excitation point corresponding to different normal load level of the plate by using branch modal synthesis. *N* denotes the normal load applied on the dry friction contact.

in agreement with the result obtained with the full order system, as shown in Fig. 35. However, it should be acknowledged that there is disparity in frequency and amplitude between the reduced model and the full model, more precisely 10% in frequency and 2% in the peak amplitude of the first resonance when the normal loads is equal to 0.05 N. Choosing more modes can certainly increase the accuracy of the reduced model at the price of computational efficiency, thus a compromise should be made. An important observation is that, even if there is a discrepancy in frequency, peak amplitude and maximal damping factor, the optimal normal load ensuring optimal damping remains the same.

To sum up, all three cases show that steady state responses obtained with the modal synthesis method agree with those obtained with Newmark-β and HBM methods. Traditional methods are hindered by the need to handle a very large number of harmonics or a large model to accurately describe the nonlinear contact force, whereas the modified method presented here achieves acceptable accuracy at much lower cost. The numerical results, including forced responses and modal parameters as a function of modal amplitude, provide a clear picture of the behavior of such elements and their differences in the case of different normal loads and different dry friction models. The efficiency and the speed of the method allow studying the optimal normal load that should be applied on the friction damper.

5. Conclusions

This paper presented a simple and efficient nonlinear modal synthesis approach to analyze the dynamic behavior of assembled structures including friction devices.

By introducing a generalized Masing model to describe the frictional device's behavior, the harmonic components of frictional force in steady state can be easily obtained using the hysteresis curve. This avoids the evaluation of friction force in the time domain and keeps the entire process in the frequency domain. The nonlinear components can therefore be directly integrated in the modal synthesis approach, permitting considerable time saving. Nonlinear modal synthesis combined with the branch modes method is shown to be more efficient for analyzing assembled systems.

The frictional damping ratio is obtained by both the energetic method based on real modes and the complex modal synthesis method. The nonlinear dynamics of the system is described from a modal standpoint, by studying the variation trends of nonlinear modal parameters, in other words the natural frequency and frictional damping ratio as a function of modal amplitude.

The proposed method was applied to three systems from the 2-dofs system to the assembled system. The results were compared with those obtained with the Newmark-β and HBM methods, and we found that the proposed method was much faster without any loss of accuracy. These three case studies proved the efficiency of the methodology presented, and its considerable potential for use in the optimization or predesign process of large engineering systems.

Acknowledgments

The work program is ongoing in the context of OpenLab PSA "VAT@Lyon".

References

[1] E. Berger, Friction modeling for dynamic system simulation, Appl. Mech. Rev. 55 (6) (2002) 535, https://doi.org/10.1115/1.1501080, ISSN 00036900.
[2] L. Gaul, R. Nitsche, The role of friction in mechanical joints modeling issues, ASME 54 (2001).
[3] C. Joannin, B. Chouvion, F. Thouverez, J.-P. Ousty, M. Mbaye, A non linear component mode synthesis method for the computation of steady-state vibrations in non-conservative systems, Mech. Syst. Signal Process. 83 (2017) 75–92.
[4] F. Pichler, W. Witteveen, P. Fischer, A complete strategy for efficient and accurate multibody dynamics of flexible structures with large lap joints considering contact and friction, Multibody Syst. Dyn. 40 (4) (2017) 407–436, https://doi.org/10.1007/s11044-016-9555-2.
[5] V. Geffen, A Study of Friction Models and Friction Compensation, Technical report Department Mechanical Engineering, 2009.
[6] O.J. Poudou, Modeling and Analysis of the Dynamics of Dry-friction-damped Structural Systems, PhD thesis University of Michigan, 2007.
[7] P.R. Dahl, A Solid Friction Model. Technical Report, The Aerospace Corporation, 1968.
[8] L. Freidovich, A. Robertsson, A. Shiriaev, LuGre-model-based friction compensation, Mechatronics 19 (1) (2009) 535–547.
[9] V. Lampaert, J. Swevers, F. Al-bender, Modification of the Leuven integrated friction model structure, IEEE Trans. Automat. Contr. 47 (4) (2002) 683–687.
[10] I.I. Argatov, E.A. Butcher, On the Iwan models for lap-type bolted joints, Int. J. Non Lin. Mech. 46 (2) (2011) 347–356, https://doi.org/10.1016/j.ijnonlinmec.2010.09.018, ISSN 00207462.
[11] L.E. Goodman, Material Damping and Slip Damping. Shock and Vibration Handbook, 19761–29.
[12] N. Peyret, J.-L. Dion, G. Chevallier, P. Argoul, Micro-slip induced damping in planar contact under constant and uniform normal stress, Int. J. Appl. Mech. (2012) https://doi.org/10.1142/S1758825110000597, April.
[13] J. Bastien, M. Schatzman, C.-H. Lamarque, Study of some rheological models with a finite number of degrees of freedom, Eur. J. Mech. A Solids 19 (2) (2000) 277–307, https://doi.org/10.1016/S0997-7538(00)00163-7.
[14] R. Bouc, Forced vibration of mechanical systems with hysteresis, In: Proceedings of Fourth Conference ICNO, 1967, pp. 2601–2608, Prague.
[15] P.M.M. Duhem, G.A. Oravas, The Evolution of Mechanics, Springer Netherlands, 1980.
[16] M.A. Krasnoselskii, A.V. Pokrovskii, Systems with Hysteresis, Springer-Verlag, New York, 1989.
[17] P. Krejč, J.P. O'Kane, A. Pokrovskii, D. Rachinskii, Properties of solutions to a class of differential models incorporating Preisach hysteresis operator, Phys. D Nonlinear Phenom. 241 (2012) 2010–2028, https://doi.org/10.1016/j.physd.2011.05.005, ISSN 01672789.
[18] D.-Y. Chiang, The generalized Masing models for deteriorating hysteresis and cyclic plasticity, Appl. Math. Model. 23 (1999) 847–863, https://doi.org/10.1016/S0307-904X(99)00015-3, ISSN 0307904X.
[19] R. Fougeres, F. Sidoroff, The evolutive masing model and its application to cyclic plasticity and ageing, Nucl. Eng. Des. 114 (1989) 273–284.
[20] G. Masing, Eigenspannungen und Verfestigung beim Messing, In: Proceedings of the Second International Congress of Applied Mechanics, 1926, pp. 332–335, Prague.
[21] W.E.W. Ferri, al, Displacement-dependent dry friction damping of a beam-like structure, J. Sound Vib. 198 (1996) 313–329, https://doi.org/10.1006/jsvi.1996.0572, ISSN 0022460X.
[22] H.P. Gavin, Numerical Integration in Structural Dynamics, Technical report Department of Civil & Environmental Engineering, Duke University, 2014.
[23] U.M. Ascher, L.R. Petzold, Computer Methods for Ordinary Differential Equations and Differential-algebraic Equations, Society for Industrial and Applied Mathematics, 1998.
[24] S. Karkar, B. Cochelin, C. Vergez, A comparative study of the harmonic balance method and the orthogonal collocation method on stiff nonlinear systems, J. Sound Vib. (2014).
[25] J.-J. Sinou, B. Petitjean, An adaptive harmonic balance method for predicting the nonlinear dynamic responses of mechanical systems - application to bolted structures, J. Sound Vib. 329 (2010) 4048–4067, https://doi.org/10.1016/j.jsv.2010.04.008.
[26] R.M. Rosenberg, The Normal Modes of Nonlinear N-Degree-of-Freedom Systems, ASME, 1962.
[27] M.E. King, A.F. Vakakis, An energy-based formulation for computing nonlinear normal modes in undamped continuous systems, J. Vib. Acoust. 116 (1993) 332–340.
[28] D. Jiang, C. Pierre, S.W. Shaw, Nonlinear normal modes for vibratory systems under harmonic excitation, J. Sound Vib. 288 (4–5) (2005) 791–812.
[29] C. Touzé, M. Amabili, Nonlinear normal modes for damped geometrically nonlinear systems: application to reduced-order modelling of harmonically forced structures, J. Sound Vib. 298 (2006) 958–981.
[30] J. Awrejcewicz, I.V. Andrianov, L.I. Manevitch, Asymptotic Approaches in Nonlinear Dynamics: New Trends and Applications, Springer Berlin/Heidelberg, 1998.
[31] X.-R. Huang, L. Jézéquel, S. Besset, L. Lin, Synthèse Modale Non-linéaire Pour l ' Analyse des Systèmes Complexes, In: CFA/VISHNO 2016, 2016b, pp. 2601–2608, Le Mans.
[32] L. Jézéquel, C. Lamarque, Analysis of non-linear dynamical systems by the normal form theory, J. Sound Vib. 149 (3) (1991) 429–459.
[33] W. Szemplinska-Stupnicka, The resonant vibration of homogeneous non-linear systems, Int. J. Non Lin. Mech. 15 (4–5) (1980) 407–415, ISSN 00207462.
[34] A.H. Nayfeh, D.T. Mook, Nonlinear Oscillations, John Wiley & Sons, 1979.
[35] F.A. Lülf, D.-M. Tran, R. Ohayon, Reduced bases for nonlinear structural dynamic systems: a comparative study, J. Sound Vib. 332 (15) (jul 2013) 3897–3921.
[36] H. Festjens, G. Chevallier, J.L. Dion, Nonlinear model order reduction of jointed structures for dynamic analysis, J. Sound Vib. 333 (7) (2014) 2100–2113, https://doi.org/10.1016/j.jsv.2013.11.039, ISSN 0022-460X.
[37] M. Mohammadali, H. Ahmadian, Efficient model order reduction for dynamic systems with local nonlinearities, J. Sound Vib. 333 (6) (2014) 1754–1766, https://doi.org/10.1016/j.jsv.2013.11.006, ISSN 0022-460X.
[38] R. Ohayon, C. Soize, Clarification about component mode synthesis methods for substructures with physical flexible interfaces, Int. J. Aeronaut. Space Sci. 15 (2) (2014) 113–122, https://doi.org/10.5139/IJASS.2014.15.2.113, ISSN 20932480.
[39] S. Besset, L. Jézéquel, Dynamic substructuring based on a double modal analysis, J. Vib. Acoust. 130 (1) (2008)011008https://doi.org/10.1115/1.2346698, ISSN 07393717.
[40] X.-R. Huang, L. Jézéquel, S. Besset, L. Lin, Optimization of the dynamic behavior of vehicle structures by means of passive interface controls, J. Vib. Contr. (2016a).

[41] L. Jézéquel, H.D. Setio, Component modal synthesis methods based on hybrid models, Part I: theory of hybrid models and modal truncation methods, ASME. J. Appl. Mech. (1994) 100–108, https://doi.org/10.1115/1.2901383.
[42] E. Chatelet, G. Michon, L. Manin, G. Jacquet, Stick/slip phenomena in dynamics: choice of contact model. Numerical predictions & experiments, Mech. Mach. Theor. 43 (10) (2008) 1211–1224, https://doi.org/10.1016/j.mechmachtheory.2007.11.001, ISSN 0094114X.
[43] F. Al-Bender, Fundamentals of friction modelling, In: ASPE Spring Topical Meeting on Control of Precision Systems, 2010, pp. 117–122, https://doi.org/10.1361/asmhba000, ISSN 0036-8733.
[44] M. Schatzman, Numerical Analysis: a Mathematical Introduction, Clarendon Press, 2002.
[45] R.R. Craig, M.C.C. Bampton, Coupling of substructures for dynamics analyses, AIAA J. 6 (7) (1968) 1313.
[46] T.K. Caughey, Equivalent linearization techniques, J. Acoust. Soc. Am. 34 (12) (2001) 1962, https://doi.org/10.1121/1.1937120, ISSN 00014966.
[47] L. Jézéquel, Structural damping by slip in joints, ASME J. Vib. Acoust. Stress Reliab. Des. 105 (3) (1983) 497–504.
[48] J. Bastien, F. Bernardin, C.-H. Lamarque, Non Smooth Deterministic or Stochastic Discrete Dynamical Systems. Applications to Models with Friction or Impact, Wiley-ISTE, 2013.
[49] M. Agnieszka, Rotordynamics, CRC Press, 2005.